Pseudopotential-based multiband k·p method for ~250 000-atom nanostructure systems

Lin-Wang Wang* and Alex Zunger
National Renewable Energy Laboratory, Golden, Colorado 80401
(Received 4 June 1996)

The electronic structure of quantum wells, wires, and dots is conventionally described by the envelope-function eight-band **k·p** method (the ''standard **k·p** model'') whereby coupling with bands other than the highest valence and lowest conduction bands is neglected. There is now accumulated evidence that coupling with other bands and a correct description of far-from-Γ bulk states is crucial for quantitative modeling of nanostructure. While multiband generalization of the **k·p** exists for *bulk* solids, such approaches for *nanostructures* are rare. Starting with a pseudopotential plane-wave representation, we develop an efficient method for electronic-structure calculations of nanostructures in which (i) multiband coupling is included throughout the Brillouin zone and (ii) the underlying bulk band structure is described correctly even for far-from-Γ states. A previously neglected interband overlap matrix now appears in the **k·p** formalism, permitting correct intervalley couplings. The method can be applied either using self-consistent potentials taken from *ab initio* calculations on prototype *small* systems or from the empirical pseudopotential method. Application to both short- and long-period $(GaAs)_p/(AlAs)_p$ superlattices (SL) recovers (i) the bending down (''deconfinement'') of the $\Gamma(\Gamma)$ energy level of (001) SL at small periods p; (ii) the type-II–type-I crossover at $p \approx 8$ SL, and (iii) the even-odd oscillation of the energies of the $R/X(L)$ state of (001) SL and $\Gamma(L)$ state of (111) SL. Introducing a few justified approximations, this method can be used to calculate the eigenstates of physical interest for large nanostructures. Application to spherical GaAs quantum dots embedded in an AlAs barrier (with ~250 000 atoms) shows a type-II–type-I crossover for a dot diameter of 70 Å, with an almost zero Γ-X repulsion at the crossing point. Such a calculation takes less than 30 min on an IBM/6000 workstation model 590. [S0163-1829(96)03439-X]

I. INTRODUCTION: THE NEED FOR A BETTER k·p METHOD FOR NANOSTRUCTURES

Most electronic-structure calculations of semiconductor nanostructures are performed today using the ''standard model,'' namely, the four-band (eight-band, including spin) **k·p** envelope-function approach.[1–8] In this approach the electronic states ψ^{NS} of the nanostructure (NS) are expanded in the zero-wave-vector (Γ-point) Bloch wave functions $u_{n,\Gamma}(r)$ of the underlying bulk solids and the expansion coefficients $F_n(r)$ (''envelope functions'') for band index n are assumed to be slowly varying spatial functions. Thus

$$\psi^{NS}(r)=\sum_{n=1}^{N_b} F_n(r)u_{n,\Gamma}(r)\equiv\sum_{n=1}^{N_b}\left\{\sum_{\mathbf{k}} b_{n,k}e^{i\mathbf{k}\cdot\mathbf{r}}\right\}u_{n,\Gamma}(r), \tag{1}$$

where the sum over the wave vector **k** extends over the first Brillouin zone (BZ) of the underlying crystal. In the standard model, the sum over bands n includes the top three valence bands and the single lowest conduction band. While extensions of the **k·p** method to include many bands ($N_b \geqslant 4$) have appeared for *bulk* solids,[3,9,10] practical multiband approaches for *nanostructures* are rare and difficult to implement.[7,11,12]

While eminently successful in describing states in wide ($\geqslant$100 Å) quantum wells, the standard model encounters some limitations in short-period superlattices, films, and dots. These limitations can be appreciated by contrasting its predictions with those of the more exact ''direct diagonalization'' approach.[13–19] In the latter approach one expands the wave function in a large basis of plane waves

$$\psi^{NS}(r)=\sum_{\mathbf{k}}^{N_k} C_k e^{i\mathbf{k}\cdot\mathbf{r}} \tag{2}$$

and solves the single-particle equation for the nanostructure atomistic potential $V^{NS}(r)$,

$$\left\{-\frac{1}{2m_0}\nabla^2+V^{NS}(r)\right\}\psi^{NS}(r)=\epsilon^{NS}\psi^{NS}(r). \tag{3}$$

Using efficient algorithms,[13,14] it permits applications to $O(10^3)$ atom nanostructures. Unlike Eq. (1), the sum over **k** in Eq. (2) is not restricted to the BZ. Unlike the standard model, this ''plane-wave basis direct diagonalization approach'' permits coupling between all bands and is able to describe the bulk band structure throughout the BZ, not just near one special **k** point. Such direct single-particle calculations of the electronic properties of small quantum structures (superlattices, films, and dots) have produced features that escaped the standard four-band **k·p** approach. For (001) $(GaAs)_p/(AlAs)_p$ *superlattices*, these include (i) the even-odd oscillations[15,16] of the energies of the L-folded states $R(L)$ and $X(L)$ with the period p, (ii) the *redshift*[15,16] (''deconfinement'') of the $\Gamma(\Gamma)$ conduction band at short periods, (iii) the interaction, repulsion, and crossing of the two lowest conduction bands $\Gamma(\Gamma)$ and $\Gamma(X_z)$ (Γ folded and X_z folded, respectively) at a critical superlattice period $p_c \sim 8-11$,[16] (iv) the significant *quantitative* overestimation by the standard model of the position of the $\Gamma(\Gamma)$ conduction band with

respect to direct diagonalization,[16] (v) significant *quantitative* underestimation by the standard model of the position of the second heavy-hole state (hh2) and split-off bands for binding energies $\geqslant$ 200 meV[16], and incorrect out-of-plane dispersion and incorrect position p of the avoided crossing,[16] (vi) omission of the spin splitting for the in-plane dispersion of the valence bands, and (vii) overestimation of the mass anisotropy $m_{\parallel}/m_{\perp}$ at Γ for both electrons and holes.[16]

While it was generally expected[4] that the standard model will fail for small nanostructures (e.g., short-period superlattices), direct diagonalization studies[16] have shown that the situation is not so simple. For example, the first heavy-hole (hh1) and the first light-hole (lh1) valence-band energies of $(\mathrm{GaAs})_p/(\mathrm{AlAs})_p$ (001) superlattices are accurately described by the standard model even down to the $p=1$ monolayer superlattice limit, while the conduction bands folded from Γ and X are poorly described even at $p\approx 20$. This is so because the standard $\mathbf{k}\cdot\mathbf{p}$ model describes poorly the energy of the zinc-blende X_{1c} state which has a significant projection in the superlattice conduction band. On the other hand, the coupling between the folded X_{1v} and Γ_{15v} states at the superlattice *valence* band (also described poorly) happens to be weak, so its misrepresentation is inconsequential. Incorrect description of intervalley coupling of folded states is also the reason for the significant errors made by the $\mathbf{k}\cdot\mathbf{p}$ model in describing the values of the superlattice miniband effective-mass tensor, the deformation potential,[17] and the wave-function localization[18] of InP/GaP superlattices.

In isolated GaAs or Si quantum *films*, the direct diagonalization approach reveals a thickness-independent ''zero confinement state'' at the valence-band maximum,[19] which is missed by the standard $\mathbf{k}\cdot\mathbf{p}$ model. Furthermore, in isolated quantum *dots* of Si and CdSe,[20–22] accurate description of the observed band gap vs size dependence requires a many-band approach.

Common to all of the failures of the standard model are (i) the neglect of intervalley (e.g., Γ-X) couplings and (ii) the poor description of the bulk band structure over most of the first Brillouin zone. While both goals can be accomplished by the plane-wave direct diagonalization approach using a pseudopotential description of the nanostructure potential $V^{\mathrm{NS}}(r)$ [Eqs. (2) and (3)], the number N_k of the plane-wave basis functions increases in this approach too rapidly with system size. More importantly, there is no simple physical principle (other than a systematic change of N_k) telling us how to reduce the size of the basis set without introducing a significant error. Thus only $O(10^3)-O(10^4)$ atom systems can be conveniently described, even using linear-in-size matrix diagonalization techniques in which only eigenvalues in a desired energy window are sought.[14] There are some important questions in nanostructure physics that require consideration of larger numbers of atoms. For example, while in (i) (001) $(\mathrm{AlAs})_p/(\mathrm{GaAs})_p$ *superlattices*, the type-II–type-I transition occurs at[23] $p_c\sim 8-11$ (32–44 atoms/supercell), and in (ii) AlAs-embedded GaAs *wire* it occurs at the diameter $D\geqslant 52$ Å ($\sim$2000 atoms/supercell), in (iii) AlAs-embedded GaAs *dots*, this transition is estimated to occur at $D\geqslant 70$ Å ($\sim$250 000 atoms/supercell), well outside the reach of direct diagonalization approach. The representation of Eq. (1) (where bulk Bloch functions $\{u_{n,\Gamma}\}$ are used instead of individual plane waves) is more attractive for such 10^4-10^6 atom systems, since in this limit the number of basis functions used to describe the envelope function $F_n(r)$ can be *system-size independent*. More specifically, one could limit the sum to those (n,k) values that are physically needed to give good convergence, rather than using all states. However, the standard $\mathbf{k}\cdot\mathbf{p}$ method cannot be used here since it does not describe the Γ and X states together, hence it cannot describe their couplings. Thus one must find effective ways to include couplings between energetically close bulk bands and to describe correctly the bulk band structure in the full BZ, not just near Γ.

In this paper, we present an efficient method, that extends the current four-band $\mathbf{k}\cdot\mathbf{p}$ model to an N_b-band model. The method accurately describes the band structure over the whole BZ and allows couplings between states of different BZ valleys. We find that $N_b=15$ bands (30 with spin) is adequate in most cases. Our formalism is different from the standard $\mathbf{k}\cdot\mathbf{p}$ formalism in that (i) the value of $\mathbf{k}$ in the second equality of Eq. (1) is not required to be close to Γ and (ii) intervalley coupling, (e.g., between Γ and X) is presented.

As an illustration of our method, we have applied it to an $\sim$ 250 000-atom system consisting of a GaAs quantum dot embedded in an AlAs matrix. The critical diameter for the Γ-X crossing is found to be 70 Å. This calculation takes less than 30 min on an IBM 6000/590 workstation for each quantum dot. That this is a relatively short computational time can be appreciated by noting that even using the standard model, calculation of a three-dimensional nanostructure poses a difficult computational task.[6]

II. THE GENERAL MANY-BAND k·p FORMALISM

A. Bulk crystals

Consider first a pure crystal A with a local periodic potential $V^A(r)$ and Hamiltonian $\hat{H}^A=-(1/2m_0)\nabla^2+V^A$. The single-particle equation is

$$\hat{H}^A\psi^A_{nk}(r)=\epsilon^A_{nk}\psi^A_{nk}(r), \tag{4a}$$

where

$$\psi^A_{nk}(r)\equiv u^A_{nk}(r)e^{i\mathbf{k}\cdot\mathbf{r}}. \tag{4b}$$

Since $\{u^A_{nk}(r)\}$ for $k=0$ is a complete basis set, we can expand the $k\neq 0$ wave functions by the $k=0$ basis (''u_0 representation'') as

$$\psi^A_{nk}(r)=\sum_m^{N_b} b_m(nk)\left|u^A_{m,0}e^{i\mathbf{k}\cdot\mathbf{r}}\right\rangle. \tag{5}$$

Inserting (5) into Eq. (4) and using $\hat{H}^A u^A_{n,0}=\epsilon^A_{n,0}u^A_{n,0}$ we find the secular equation

$$\sum_m^{N_b}\{H^A(n,m,k)-\delta_{n,m}\epsilon^A_{p,k}\}b_m(pk)=0. \tag{6}$$

Here p is the band index and the Hamiltonian matrix element is

$$H^A(n,m,k)=\left[\epsilon^A_{n,0}+\frac{k^2}{2m_0}\right]\delta_{n,m}-i\mathbf{k}\cdot\mathbf{P}^A(n,m), \tag{7}$$

where m_0 is the real electron mass. The momentum matrix element is

$$P^A(n,m)=\langle u^A_{m,0}|\nabla|u^A_{n,0}\rangle. \tag{8}$$

Thus, given the $k=0$ eigenvalues $\{\epsilon^A_{n,0}\}$ and the $k=0$ momentum matrix $\{P^A(n,m)\}$ one can solve Eq. (6) and find the full $k\neq 0$ dispersion relation $\epsilon^A_{n,k}$ over the first BZ.

Due to the completeness of the basis $u^A_{n,0}$, we have

$$\hat{H}^A|u^A_{n,0}e^{i\mathbf{k}\cdot\mathbf{r}}\rangle=\sum_{m=1}^{N_m} H^A(n,m,k)|u^A_{m,0}e^{i\mathbf{k}\cdot\mathbf{r}}\rangle. \tag{9}$$

Here N_m is introduced for future use in Sec. III. For now $N_m=N_b=\infty$. If $N_m\neq\infty$, Eq. (9) is only an approximation.

B. Nanostructures

Consider now a heterostructure (superlattice, embedded quantum dot, etc.) consisting of material A and material B. We will assume that A and B have the same lattice period R and that they are in the same crystalline orientation. We further assume that the potential $V^{\rm NS}(r)$ of this nanostructure can be constructed from the periodic atomistic potentials $V^A(r)$ and $V^B(r)$ of materials A and B as

$$V^{\rm NS}_w(r)=\sum_{R\in A}^{N_c} w(r-R)V^A(r)+\sum_{R\in B}^{N_c} w(r-R)V^B(r). \tag{10}$$

The sum over the lattice vectors R runs over N_c primary cells in A and B. Each lattice vector belongs to a single primary cell and each primary cell belongs to either A or B. The crystalline potentials $V^A(r)$ and $V^B(r)$ can be obtained either from self-consistent bulk band-structure calculations[24] or from empirically fitted screened pseudopotentials.[26,25] The function $w(r-R)$ describes the spatial arrangement of material (including the A/B interface). $w(r-R)$ occupies a region of roughly one primary cell and satisfies, for any r and for $R\in A\cup B$, the relation $\Sigma_R w(r-R)=1$. This gives $\int w(r)d^3r=\Omega_c$, where Ω_c is the volume of a primary cell. Using Eq. (10), it is easy to prove that the nanostructure Hamiltonian is

$$\hat{H}^{\rm NS}=\sum_{R\in A} w(r-R)\hat{H}^A+\sum_{R\in B} w(r-R)\hat{H}^B\equiv\hat{H}^{\rm PA}+\hat{H}^{\rm PB}, \tag{11}$$

where the superscripts PA and PB stand for part A and part B, respectively.

We expand the wave functions $\psi^{\rm NS}(r)$ of the nanostructure in terms of A-type $k=0$ basis functions

$$\psi^{\rm NS}(r)=\frac{1}{\sqrt{N_c}}\sum_{n=1}^{N_b}\left\{\sum_{\mathbf{k}} b_{nk}e^{i\mathbf{k}\cdot\mathbf{r}}\right\}u^A_{n,0}(r), \tag{12}$$

where N_c is the total number of primary cells in the system, $\mathbf{k}$ is the supercell wave vector, and the sum over $\mathbf{k}$ extends over the first BZ. In this u_0 representation, the nanostructure wave function is expanded in terms of *zero-wave-vector* Bloch functions of the constituent bulk solids. The advantage of the u_0 representation is that the nanostructure Hamiltonian can be written analytically via the **k·p** formalism, thus providing insights for further analysis and approximations. The disadvantage of this approach is that many Γ-point Bloch basis functions may be needed for representing even bulk wave functions at $k\neq 0$. Thus N_b cannot be restricted to a conveniently small number. We will see, however, that the need for a relatively large value of N_b can be overcome if before the diagonalization of the secular problem we convert the u_0 representation to a u_k representation. The latter means that one replaces in Eq. (12) $u_{n,0}$ by $u_{n,k}$, namely,

$$\psi^{\rm NS}(r)=\frac{1}{\sqrt{N_c}}\sum_{n=1}^{N_b}\left\{\sum_{\mathbf{k}} b'_{nk}e^{i\mathbf{k}\cdot\mathbf{r}}\right\}u^A_{n,k}(r). \tag{13}$$

Since $u^A_{n,k}(r)e^{i\mathbf{k}\cdot\mathbf{r}}$ is the eigenstate $\psi^A_{nk}(r)$ of bulk A [Eq. (4b)], the u_k representation implies that the nanostructure wave function is written as a linear combination of bulk bands

$$\psi^{\rm NS}(r)=\frac{1}{\sqrt{N_c}}\sum_{n=1}^{N_b}\sum_{\mathbf{k}} b'_{nk}\psi^A_{nk}(r). \tag{14}$$

This approach has been used by Dandrea and Zunger[27] and by Xia and Baldereschi,[28] where superlattice wave functions were expanded using Eq. (14) with $\psi^A_{nk}(r)$ being replaced by the (virtual crystal) Bloch function of the *A-B alloy*. The advantage of this u_k representation is that the number of bands N_b can be reduced to a small value. Here we will develop the formalism using the u_0 representation (for analytical simplicity), but we will later revert to the u_k representation for computational compactness.

The secular equation for the expansion coefficients $\{b_{nk}\}$ and the nanostructure eigenvalues $\epsilon^{\rm NS}$ can be written in the u_0 representation as

$$\sum_{\mathbf{k}}\sum_{n=1}^{N_b}\{H^{\rm NS}_A(mk',nk)-\delta_{m,n}\delta_{k',k}\epsilon^{\rm NS}\}b_{nk}=0. \tag{15}$$

We will drop from now on the index ''0'' from $u_{n,0}$ unless needed explicitly. Here $H^{\rm NS}_A(mk',nk)\equiv(1/N_c)\langle u^A_m e^{i\mathbf{k}'\cdot\mathbf{r}}|\hat{H}^{\rm NS}|u^A_n e^{i\mathbf{k}\cdot\mathbf{r}}\rangle$ is the Hamiltonian matrix of $\hat{H}^{\rm NS}$ in the basis set of Eq. (12). Since $\hat{H}^{\rm NS}$ has part A and part B [Eq. (11)], we will compute the respective matrix elements separately. Applying $\hat{H}^{\rm PA}$ to the basis function of Eq. (12) and using Eq. (9) we have

$$\hat{H}^{\rm PA}|u^A_n e^{i\mathbf{k}\cdot\mathbf{r}}\rangle=\sum_{R\in A} w(r-R)\sum_{p=1}^{N_m} H^A(n,p,k)|u^A_p e^{i\mathbf{k}\cdot\mathbf{r}}\rangle. \tag{16}$$

Multiplying Eq. (16) by $\langle u^A_m e^{i\mathbf{k}'\cdot\mathbf{r}}|$, we get the matrix elements of part A of $H^{\rm NS}_A(mk',nk)$ in an A-type basis as

$$\begin{aligned}H^{\rm PA}_A(mk',nk)&\equiv\frac{1}{N_c}\langle u^A_m e^{i\mathbf{k}'\cdot\mathbf{r}}|\hat{H}^{\rm PA}|u^A_n e^{i\mathbf{k}\cdot\mathbf{r}}\rangle\\&=\sum_{p=1}^{N_m} H^A(n,p,k)S^A(p,m,k'-k)C^A(k'-k).\end{aligned} \tag{17}$$

Here the *interband overlap* in material A is

$$S^A(p,m,k)=\int u_p^A(r)u_m^{A*}(r)w(r)e^{-i\mathbf{k}\cdot\mathbf{r}}d^3r \qquad (18)$$

and the *structure factor* of material A is

$$C^A(k)=\frac{1}{N_c}\sum_{R\in A} e^{-i\mathbf{k}\cdot\mathbf{R}}. \qquad (19)$$

Note that because of the factor $w(r)\exp(-i\mathbf{k}\cdot\mathbf{r})$, we have $S^A(p,m,k)\neq\delta_{p,m}$ despite the orthonormality between u_p^A and u_m^A The same formalism gives for the matrix elements of part B of the Hamiltonian in the B-type basis set

$$H_B^{\mathrm{PB}}(mk',nk)\equiv\frac{1}{N_c}\langle u_m^B e^{i\mathbf{k}'\cdot\mathbf{r}}|\hat{H}^{\mathrm{PB}}|u_n^B e^{i\mathbf{k}\cdot\mathbf{r}}\rangle$$
$$=\sum_{p=1}^{N_m} H^B(n,p,k)S^B(p,m,k'-k)C^B(k'-k). \qquad (20)$$

In Eqs. (17) and (20), the subscripts A or B denote the basis functions, while the superscripts PA and PB denote the Hamiltonian defined in Eq. (11). Because $\{u_n^A(r)\}$ and $\{u_m^B(r)\}$ each represent a complete basis, they can be inter-transformed via a unitary transformation

$$u_n^A(r)=\sum_{m=1}^{N_b}\tilde{U}(m,n)u_m^B(r) \qquad (21)$$

and

$$\tilde{U}(m,n)=\int_{\mathrm{PC}} u_m^{B*}(r)u_n^A(r)d^3r \qquad (22)$$

where PC stands for integration over one primary cell. Thus the matrix element H_A^{PB} of the Hamiltonian $\hat{H}^{\mathrm{PB}}$ in an A-type basis of Eq. (12) can be obtained from H_B^{PB} in Eq. (20) by

$$H_A^{\mathrm{PB}}(mk',nk)\equiv\frac{1}{N_c}\langle u_m^A e^{i\mathbf{k}'\cdot\mathbf{r}}|\hat{H}^{\mathrm{PB}}|u_n^A e^{i\mathbf{k}\cdot\mathbf{r}}\rangle$$
$$=\sum_{p',p=1}^{N_b}\tilde{U}^*(p',m)H_B^{\mathrm{PB}}(p'k',pk)\tilde{U}(p,n). \qquad (23)$$

Finally, the matrix elements $H_A^{\mathrm{NS}}(mk',nk)$ in Eq. (15) of the total nanostructure Hamiltonian in an A-type basis is

$$H_A^{\mathrm{NS}}(mk',nk)\equiv\frac{1}{N_c}\langle u_m^A e^{i\mathbf{k}'\cdot\mathbf{r}}|\hat{H}^{\mathrm{NS}}|u_n^A e^{i\mathbf{k}\cdot\mathbf{r}}\rangle$$
$$=H_A^{\mathrm{PA}}(mk',nk)+H_A^{\mathrm{PB}}(mk',nk), \qquad (24)$$

where the two terms are given by Eqs. (17) and (23). Note that this $H_A^{\mathrm{NS}}(mk',nk)$ is not explicitly Hermitian because k,k' and n,m are treated differently in Eqs. (17) and (20). However, as long as $N_b=\infty$, it can be shown that $H_A^{\mathrm{NS}}(mk',nk)$ is indeed Hermitian.

We have seen that, unlike the standard model, a correct description of interband coupling requires that Eqs. (17) and (20) include an interband overlap matrix $S^{A(B)}(p,m,k)$. This matrix [Eq. (18)] has to be evaluated for all needed supercell wave vectors $\mathbf{k}$ inside a 2BZ region. This 2BZ region is a $\mathbf{k}$-space region that looks like the BZ, but is twice as large in each direction [e.g., for a fcc lattice, the boundary point of the 2BZ in the (001) and (111) directions are the $2X$ and $2L$ $\mathbf{k}$ points].

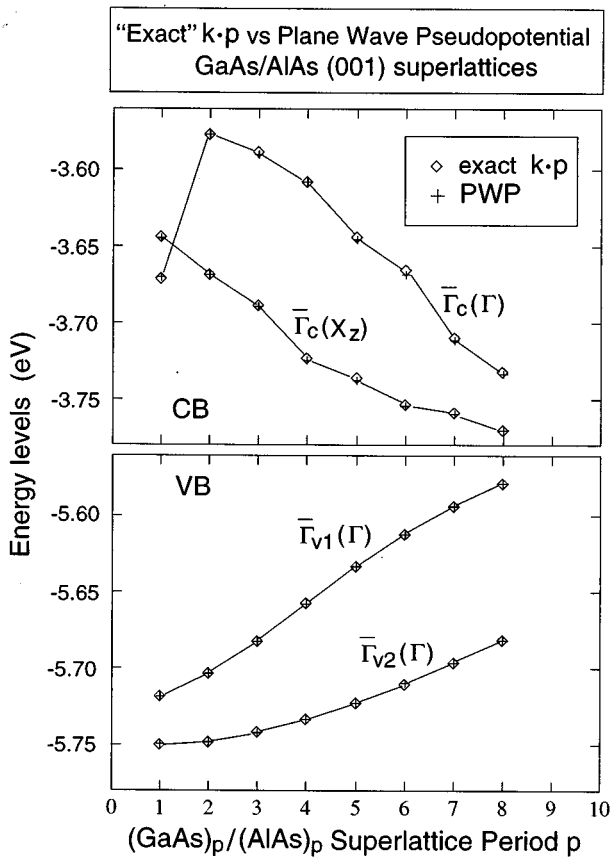

FIG. 1. Comparison of ''exact'' $\mathbf{k}\cdot\mathbf{p}$ results with direct plane-wave pseudopotential (PWP) calculations for the GaAs/AlAs (001) superlattice. The exact $\mathbf{k}\cdot\mathbf{p}$ is defined here as using $N_b=65$, $N_m=369$, and direct evaluations of $S^{A(B)}(p,m,k)$ for some $\mathbf{k}$ points. The small differences are due to interpolation of $S^{A(B)}(p,m,k)$ for the other $\mathbf{k}$ points.

In the current formalism, we have ignored the strain and spin-orbit coupling. However, such effects can be described using terms similar to those in the standard $\mathbf{k}\cdot\mathbf{p}$ model.

In summary, for nanostructure atomistic potentials of the type shown in Eq. (10), the secular equation in a Γ-like basis set of Eq. (12) is given by Eqs. (17), (23), and (24). The above formalism is exact if the number of bands N_b equals infinity. We now study the effects of finite N_b on the bulk band structure and on the energies of nanostructures.

III. FINITE-N_b ANALYSIS

There are a number of errors related to the truncation of the sum over Γ-like bands to a finite number N_b.

(a) The bulk dispersion relation $\epsilon_{p,k}^A$ of Eq. (6) is inaccurate if N_b in that equation is truncated. We refer to this as the $\mathbf{k}\cdot\mathbf{p}$ bulk band structure error.

(b) The bulk eigenfunction appearing in Eq. (9) is not satisfied if a finite $N_m=N_b$ is used. We refer to this error as

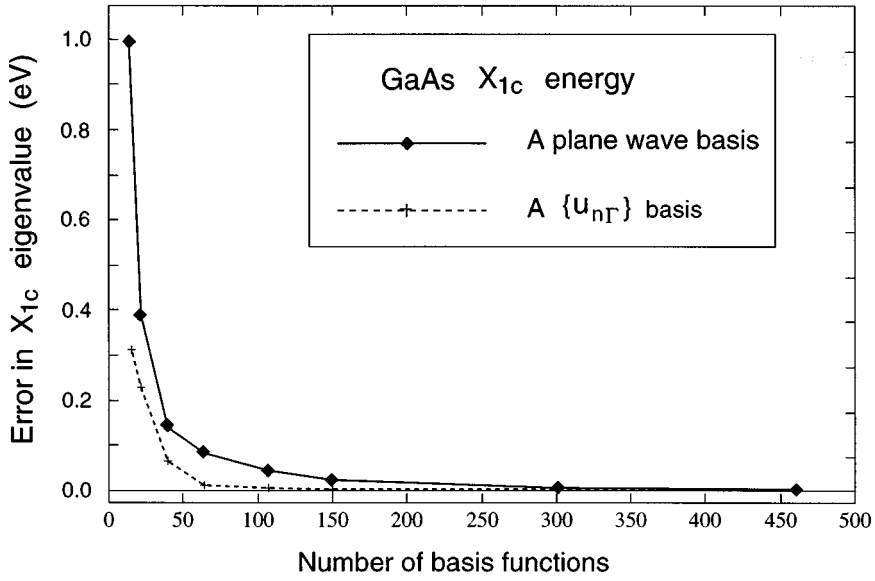

FIG. 2. Convergence of the bulk GaAs X_{1c} state energy vs the number of plane-wave basis functions (solid lines, pseudopotential calculation) and the number of $u_{n\Gamma}$ states (dashed line, **k·p** calculation).

the eigenfunction equation error.

(c) The transformation matrix $\tilde{U}(m,n)$ between $u_n^A(r)$ and $u_m^B(r)$ [Eqs. (21) and (22)] is not unitary if N_b is truncated. In this case, $\{u_n^B(r)\}$ cannot be connected exactly to $\{u_n^A(r)\}$. We refer to this as the *unitary connection error*. In what follows, we will first assess the effects of these three errors, then we will suggest ways to fix them, *within a truncated basis set*.

A. $(GaAs)_p/(AlAs)_p$ superlattices: An "exact" k·p result

Before we reduce the number of bands in the **k·p** basis, we first illustrate our exact **k·p** formalism of Sec. II for $(GaAs)_p/(AlAs)_p$ (001) superlattices. This will be used as a benchmark for subsequent approximations. We consider a superlattice with an abrupt interface, which means that in Eq. (10) we have $w(z)=1/|R|$ for $-R/2<z<R/2$ and zero elsewhere [z is the (001) coordinate]. The potential $V_w^{\rm NS}$ generated from Eq. (10) (in which V^A and V^B are superpositions of screened atomic pseudopotentials[25]) is used as the input potential for the plane-wave direct diagonalizations.

To get an exact result (i.e., equal to the direct plane-wave diagonalization), the three **k·p** errors (a)–(c) noted above must first be removed. To this end, we have taken a few special treatments in our **k·p** implementations and in the plane-wave calculations.

First, we have used a special polyhedron zone [described in Appendix A (Ref. 26)] to select the plane-wave basis in the plane-wave direct diagonalization calculations. (This zone is only used in this section for the current purpose of comparison.) There are 65 basis functions and 65 Bloch bands and we have used all of them in our **k·p** calculation, so $N_b=65$. This special zone method ensures that the plane-wave basis set will not change when the **k** point moves insides the first BZ. As a result, the $N_b=65$ **k·p** band structure is exactly the same as the direct diagonalization plane-wave band structure. This removes the band structure error (a). The use in our **k·p** method of all the Γ Bloch states available in a given plane-wave calculation also removes the unitary connection error (c).

Second, to avoid the eigenfunction equation error (b), we have used $N_m \gg N_b$ in Eqs. (9) and (17). (In practice, we have used $N_m=369$, which gives a well-converged result.) The **k·p** Hamiltonian matrix $H_A^{\rm NS}$ is defined by Eqs. (24), (23), (20), and (17). The $S^{A(B)}(p,m,k)$ matrix is evaluated directly by its definition of Eq. (18) for some **k** points and via interpolations for other **k** points.

The exact **k·p** results for the superlattice are shown in Fig. 1 where they are compared with the results of plane-wave direct diagonalizations. The two results are the same, except for very small errors introduced by the interpolation of the $S^{A(B)}(p,m,k)$ matrix. This establishes an exact **k·p** method whose results equal those obtained in a direct plane-wave diagonalization.

B. k·p for bulk GaAs: Truncated expansion

We will now systematically reduce the number of bands N_b to see the effects on the **k·p** bulk band structures. Figure 2 depicts the error in the X_{1c} band energy of bulk GaAs as a function of (i) the number N_k of individual plane waves in the expansion of Eq. (2) and, independently, (ii) the number N_b of Γ-point Bloch functions in the **k·p** expansion of Eqs. (6) and (7). In both cases, we use the local empirical pseudopotential fitted recently[25] to bulk GaAs. To obtain solutions of the **k·p** problem of Eqs. (5) and (6), we first performed a converged plane-wave pseudopotential Γ-point bulk calculation, obtaining $\{u_n^A(r)\}$, $\{\epsilon_{n,0}^A\}$, and $\{P^A(n,m)\}$. These quantities are then used in Eqs. (6) and (7) to solve the **k·p** problem. We see from Fig. 2 that reducing the bulk band structure error to 1 meV requires $\sim$ 500 plane waves in the expansion of Eq. (2) (Ref. 29) or 150 Γ Bloch bands in the expansion of Eq. (5). Use of only $\sim$10 Bloch bands gives an error of 300 meV. For applications to large nanostructures, it would be desirable to reduce N_b to a small value, say, to 10–20 bands, while keeping the error below, say, 5 meV.

We next examine the **k·p** band structure of bulk GaAs throughout the zone (not just X_{1c} as in Fig. 2), as obtained with different basis sizes. The results (Figs. 3 and 4) show that when $N_b \geqslant 15$ the **k·p** band structure is qualitatively

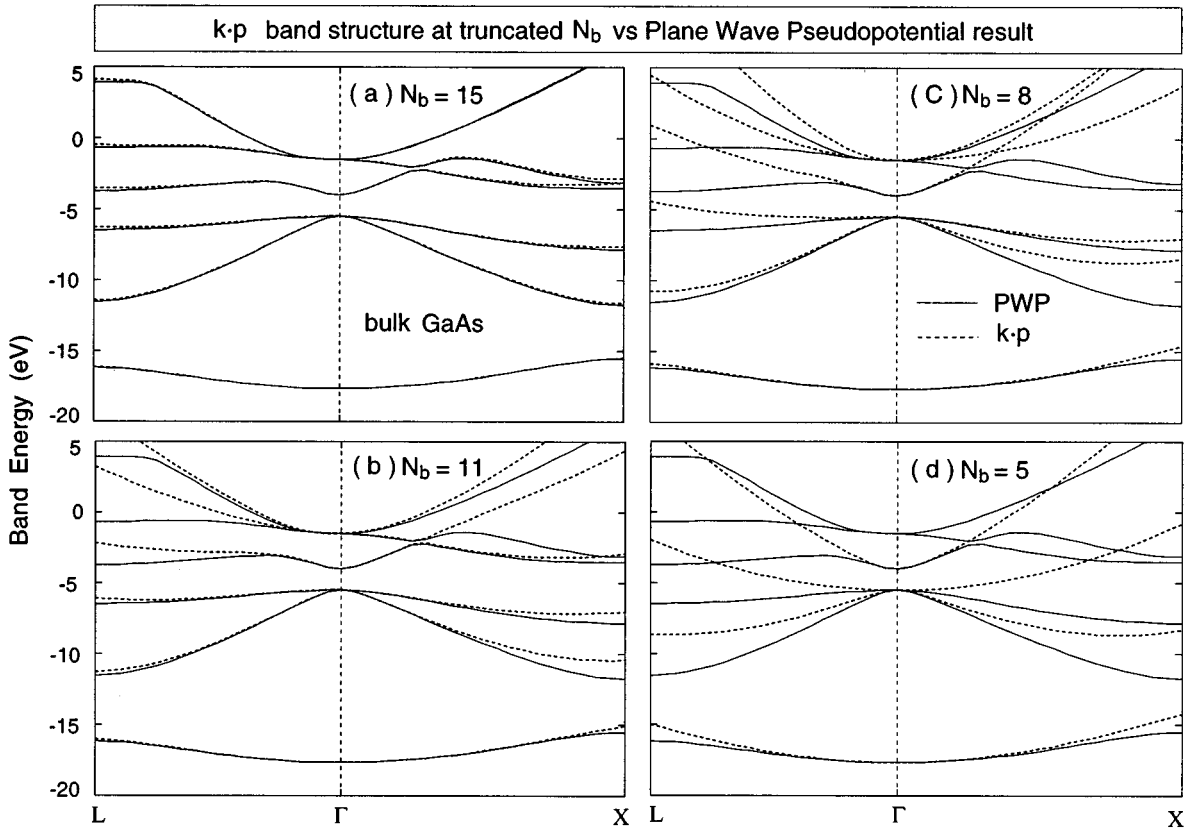

FIG. 3. Comparison of bulk GaAs $\mathbf{k}\cdot\mathbf{p}$ band structure with different number N_b of Γ-like basis functions (dashed lines). The solid lines are the $N_b=65$ results, which equal the plane-wave results using the polyhedron zone of Appendix A.

similar to that obtained by exact direct diagonalization, but that when less than 15 Γ Bloch bands are used, the band structure suddenly becomes much worse. Note in particular how for 8 or 5 Γ bands the energy of the X_{1c} band as obtained in $\mathbf{k}\cdot\mathbf{p}$ is $\sim$20 eV too high and the curvature (hence effective mass) of the valence band reverses sign. The situation is similar for AlAs and Si (not shown).

To show how many Γ Bloch states $\{u_{n\Gamma}\}$ are needed to describe the directly calculated X Bloch state u_{nX} of bulk GaAs, we plot in Fig. 5 the closure quantity

$$P_n(N_b)=\sum_{m=1}^{N_b}|\langle u_{m\Gamma}|u_{nX}\rangle|^2 \tag{25}$$

for $n=1,\ldots,8$, where $n=1$ is the lowest X_{1v} valence band, $n=4$ is the highest X_{3v} valence band, and $n=5,6,7,8$ are the lowest four conduction bands, respectively. Here $P_n(N_b)=1$ means that the nth X-point Bloch state can be described exactly by the first N_b Γ-point Bloch states. As we can see from Fig. 5, there is a sudden drop of $P_n(N_b)$ for N_b less than 15. This is consistent with the band-structure results in Figs. 3 and 4. The situation is qualitatively similar for AlAs and Si (not shown). We conclude that 15 zero-wave-vector bulk bands (30 with spin) are needed for a *qualitatively* correct description of the dispersion relation in bulk solids, while about 150 bands are needed for a *quantitatively* converged ($\leqslant 1-2$ meV) description. We will eventually [Sec. IV A] find ways to obtain a *quantitative* description using only 15 bands.

C. $\mathbf{k}\cdot\mathbf{p}$ for $(\mathrm{GaAs})_p/(\mathrm{AlAs})_p$ superlattices: Truncated expansion

Having tested the $\mathbf{k}\cdot\mathbf{p}$ convergence for the bulk solids, we next examine how the $\mathbf{k}\cdot\mathbf{p}$ errors in the bulk lead to errors in the superlattice made of these bulk solids. As discussed at the beginning of Sec. III, $\mathbf{k}\cdot\mathbf{p}$ calculations with finite-N_b values can lead to three error types. We will focus our attention in this section on the $\mathbf{k}\cdot\mathbf{p}$ band-structure error (a). As in Sec. III A, in this section too the eigenfunction equation error (b) will be removed by using $N_m=369$, much larger than N_b. The unitary connection error (c) cannot be removed easily. For the purpose of the comparisons made in this section, we deliberately set $\tilde{U}(n,m)=\delta_{n,m}$. Since this ansatz is now common to all N_b values, one could hope that the unitary connection error (c) could be partially canceled out when we compare results for different N_b values.

Figure 6 compares the exact $\mathbf{k}\cdot\mathbf{p}$ results [shown by pluses with $N_m=369$ and $\tilde{U}(n,m)$ of Eq. (22)] with results of (i) $N_m=65$ and $\tilde{U}(n,m)$ of Eq. (22) (diamonds) and (ii) $N_m=369$ and $\tilde{U}(n,m)=\delta_{n,m}$ (squares). In this figure, $N_b=65$ is used in all three calculations. By comparing the pluses and diamonds in Fig. 6, we can see that the eigenfunction equation error (b) for $N_m=65$ is rather small (about 3 meV). By comparing the pluses and squares, however, we see that the error caused by setting $\tilde{U}(n,m)=\delta_{n,m}$ is large, about 18 meV. [This does not mean that the typical unitary

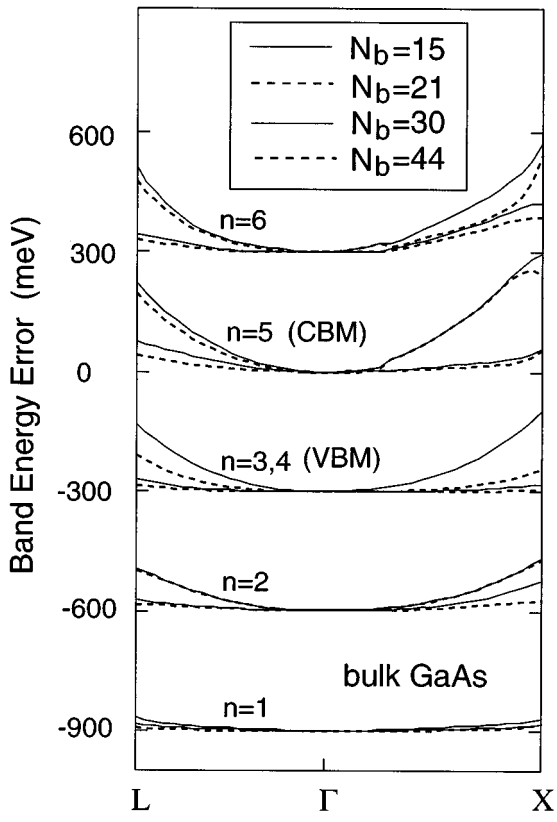

FIG. 4. Errors $\epsilon_n(N_b)-\epsilon_n(N_b=65)$ in the GaAs **k·p** band-structure energy due to reduced N_b. These errors are zero at the Γ point; the curves for different bands are shifted for clarity.

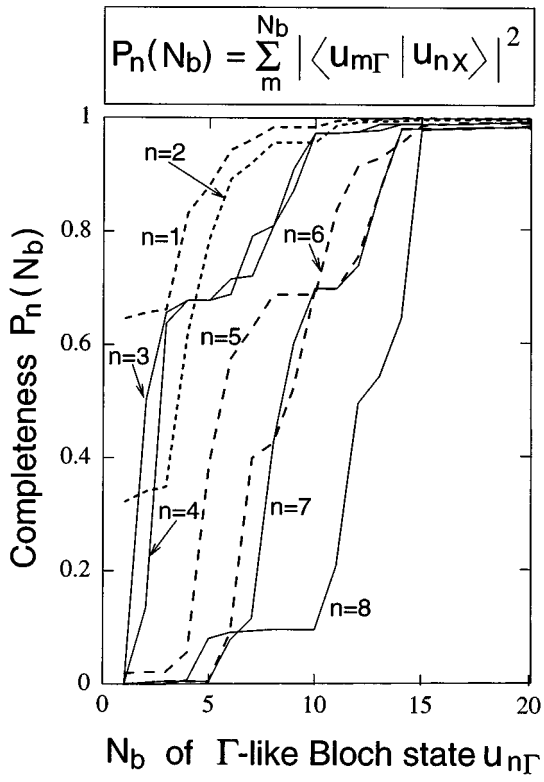

FIG. 5. Completeness $P_n(N_b)$ in describing the nth X point state in GaAs in terms of N_b Γ point basis states. $P_n=1$ means an exact description of the X point state n in terms of N_b Γ states.

connection error (c) in our final **k·p** nanostructure calculation will be ~18 meV. There, a better approximation of $\tilde{U}(n,m)$, instead of $\tilde{U}(n,m)=\delta_{n,m}$, will be used. As a result, the unitary connection error (c) will be much smaller than 18 meV.]

Convergence of **k·p** superlattice eigenvalues with N_b are shown in Figs. 7–9. Here the $N_b=65$ results serve as the references and $N_m=369$ and $\tilde{U}(n,m)=\delta_{n,m}$ are used for all calculations. When N_b changes from 65 to 44, the X-folded conduction-band $\Gamma(X_z)$ state moves up by more than 50 meV (this is consistent with the bulk band-structure errors reported in Figs. 3–4). When N_b is further reduced, the $\Gamma(X_z)$ state continues to move up. From $N_b=21$ to 15, the change is relatively small, while from $N_b=15$ to 11, the change is large. Similar trends in the error of the L-folded conduction state X/R are shown in Fig. 9. The large change below $N_b=15$ is consistent with the results found for the bulk band structure (Figs. 3 and 4) and $P_n(N_b)$ (Fig. 5). We see that the basis-set truncation error in superlattice energies parallels the errors in the bulk. The above analysis further shows that $N_b=15$ is a turning point, i.e., for $N_b<15$ Γ bands, the band structure cannot be described *even qualitatively*. Thus, in the rest of this paper, we will use $N_b=15$ Γ bands for GaAs and AlAs. We next develop a formalism appropriate to many-band coupling where a *truncated* $N_b=N_m=15$ basis set is used.

IV. THE FINITE-N_b FORMALISM

A. Fixing the k·p bulk band-structure error

The above study shows that the **k·p** error in the bulk band structure carries over to the nanostructure. So our first task here is to reduce the **k·p** bulk band-structure error (a) of band-edge states for $N_b=15$ to less than 5 meV from ~ 300 meV (see the X and L points in Figs. 3 and 4).

The effects of removing higher-energy bands on the energies of lower states can be described as Löwdin folding.[30] This is a procedure that modifies the elements of the Hamiltonian matrix so that the eigenvalues of the submatrix spanned by the lower-energy states equal the eigenvalues of the original full matrix. As a result, the effects of the truncation to finite N_b bands can be compensated by a replacement of the bare electronic mass m_0 in Eq. (7) with ''mass parameters'' m_n^A. Furthermore, to fit the dispersion in both the Γ-X and the Γ−L directions, we need a nonspherical correction term. This term comes from a higher-order Löwdin folding effect (i.e., a fourth-order term in k): $f(k)=3(k_x^4+k_y^4+k_z^4)-k^4$. [Here $f(k)=0$ for the (111) direction and $f(k)=2k^4$ for the (001) direction.] Thus we have revised Eq. (7) to

$$H^A(n,m,k)=\left[\epsilon_{n,0}^A+\frac{1}{2m_n^A}k^2+a_n^A f(k)\right]\delta_{n,m}-i\mathbf{k}\cdot\mathbf{P}^A(n,m), \tag{26}$$

where $\epsilon_{n,0}^A$ and $P^A(n,m)$ are unchanged from Eq. (7). For $N_b=15$, due to the degeneracy, we have eight independent

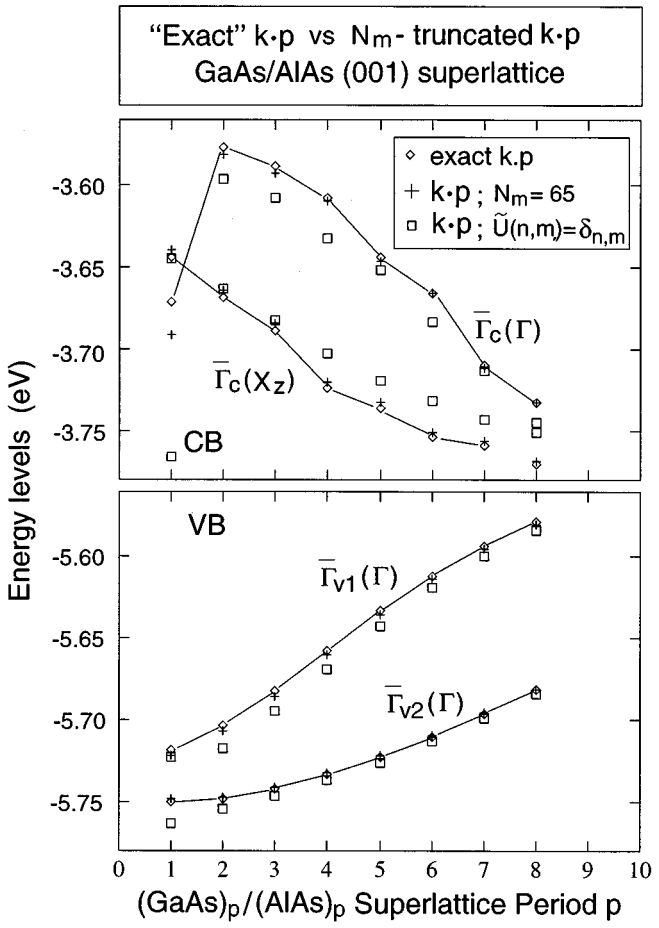

FIG. 6. Comparison between different $\mathbf{k}\cdot\mathbf{p}$ calculations using different approximations for the GaAs/AlAs (001) superlattice. The diamonds denote the exact $\mathbf{k}\cdot\mathbf{p}$ ($N_m=369$) and are the same as the diamonds in Fig. 1. Pluses truncated $N_m=65$; squares $N_m=369$, but $\tilde{U}(n,m)$ approximated as $\delta_{n,m}$. $N_b=65$ for all three calculations.

m_n^A values and eight independent a_n^A values. These are used to fit the two lowest conduction-band and the highest valence-band energies. The fitted $\mathbf{k}\cdot\mathbf{p}$ bulk band structures of GaAs and AlAs are shown in Figs. 10(a) and 10(b), while the errors, relative to a direct plane-wave diagonalization calculation, are shown in Fig. 11. The fitting parameters $m_n^{A(B)}$ and $a_n^{A(B)}$ are listed in Table I. The $m_n^{A(B)}$'s are close to 1 and the $a_n^{A(B)}$'s are small. The physically important bottom of conduction-band states ($n=5$ in Fig. 11), especially near the Γ,X,L points, have typical errors of only ~ 3 meV, much better than the unfitted error of ~ 300 meV seen in Figs. 3(a) and 4.

In this work we have calculated the quantities $\epsilon_{n,0}^A$ of Eq. (7), $P^A(n,m)$ of Eq. (9), and $S^A(n,m,k)$ of Eq. (18) using the empirical pseudopotential plane-wave method[25,26] (so as to ensure accurate eigenenergies and wave functions). These quantities can also be obtained from self-consistent calculations such as the local-density approximations (LDA) provided that the LDA errors in the band structure $\epsilon_{n,0}^A$ were subsequently corrected. If nonlocal pseudopotentials are used in the LDA or in the empirical pseudopotential calculation,[22] its effects could also be represented by the mass parameters $\{m_n\}$ and the $f(k)$ term in Eq. (26).

B. Fixing the unitary connection error

Having fixed the bulk band structure, we return now to the eigenfunction equation error (b) and unitary connection error (c). As shown in Fig. 6, the eigenfunction equation error (b) is small, at least when $N_b=N_m=65$. Thus no attempt is made to correct it here. We will use $N_b=N_m=15$ throughout the rest of the work. As also shown in Fig. 6, the unitary connection error (c) could be large if we let $\tilde{U}(n,m)$ be $\delta_{n,m}$. The $\tilde{U}(n,m)$ calculated from Eq. (22) is not unitary for truncated N_b, thus it cannot be used directly. Appendix B describes a simple procedure (Löwdin orthogonalization), with minimum modifications of $\tilde{U}(n,m)$, converting it to an unitary matrix. The resulting $\tilde{U}(n,m)$ is then used in Eq. (23). Treated in this way, the unitary connection error (c) becomes rather small.

C. A special method to calculate $S^{A(B)}(n,m,k)$

The overlap matrix $S^{A(B)}(n,m,k)$ in Eqs. (17) and (20) needs to be calculated from its definition Eq. (18) for all the nanostructure wave vector k inside the 2BZ. Direct calculation of the overlap matrix could be time consuming. For one-dimensional superlattices one can use a numerically accurate interpolation scheme as done in Sec. III. However, for three-dimensional systems (e.g., quantum dots), $S^{A(B)}(n,m,k)$ needs to be precalculated for numerous $\mathbf{k}$ values. In the following, we will introduce an alternative, easier approach to calculate this overlap matrix.

Substituting the Fourier expansion $w(r)=[\Omega_c/(2\pi)^3]\int W(k)e^{i\mathbf{k}\cdot\mathbf{r}}d^3k$ of the weight function $w(r)$ into Eq. (18) and using the fact $u_n^A(r+R)=u_n^A(r)$, we get

$$S^A(n,m,k)=\sum_G \mathcal{O}^A(n,m,G)W(k-G). \tag{27}$$

Here $\{G\}$ are the reciprocal lattice vectors of the crystal lattice vector $\{R\}$ and the overlap matrix $\mathcal{O}^A$ is defined as

$$\mathcal{O}^A(n,m,G)=\int_{\mathrm{PC}} u_n^A(r)u_m^{A*}(r)e^{-i\mathbf{G}\cdot\mathbf{r}}d^3r. \tag{28}$$

This matrix $\mathcal{O}^A(n,m,G)$ is different from the $S^A(n,m,k)$ matrix in two respects: (i) $w(r)$ is dropped from the integral in Eq. (28), and (ii) $\mathcal{O}^A$ is defined only at the reciprocal lattice $\mathbf{G}$, while S^A is defined for all supercell wave vectors $\mathbf{k}$ inside the 2BZ. If we have a smooth $w(r)$, so that its Fourier transform $W(k)$ has nonzero values only inside a finite region (e.g., inside the 2BZ), then only a finite number of $\mathbf{G}$ vectors will contribute to the summation in Eq. (27).

The overlap matrix $\mathcal{O}^{A(B)}(n,m,G)$ plays a role in the representation of the $\mathbf{k}$-space periodicity of the Bloch state in the $\mathbf{k}\cdot\mathbf{p}$ formalism. Suppose that $G=2k_X$. Then to ensure the periodicity of the Bloch function between the $-X$ and X points, $\mathcal{O}^A(n,m,2X)$ must satisfy Eq. (31) in the following. This $\mathbf{k}$-space periodicity of the Bloch states has an important practical consequence for calculations on nanostructures. In the case of X and $-X$ $\mathbf{k}$ points, we can either choose the $-X$ or the X states as basis functions, but not

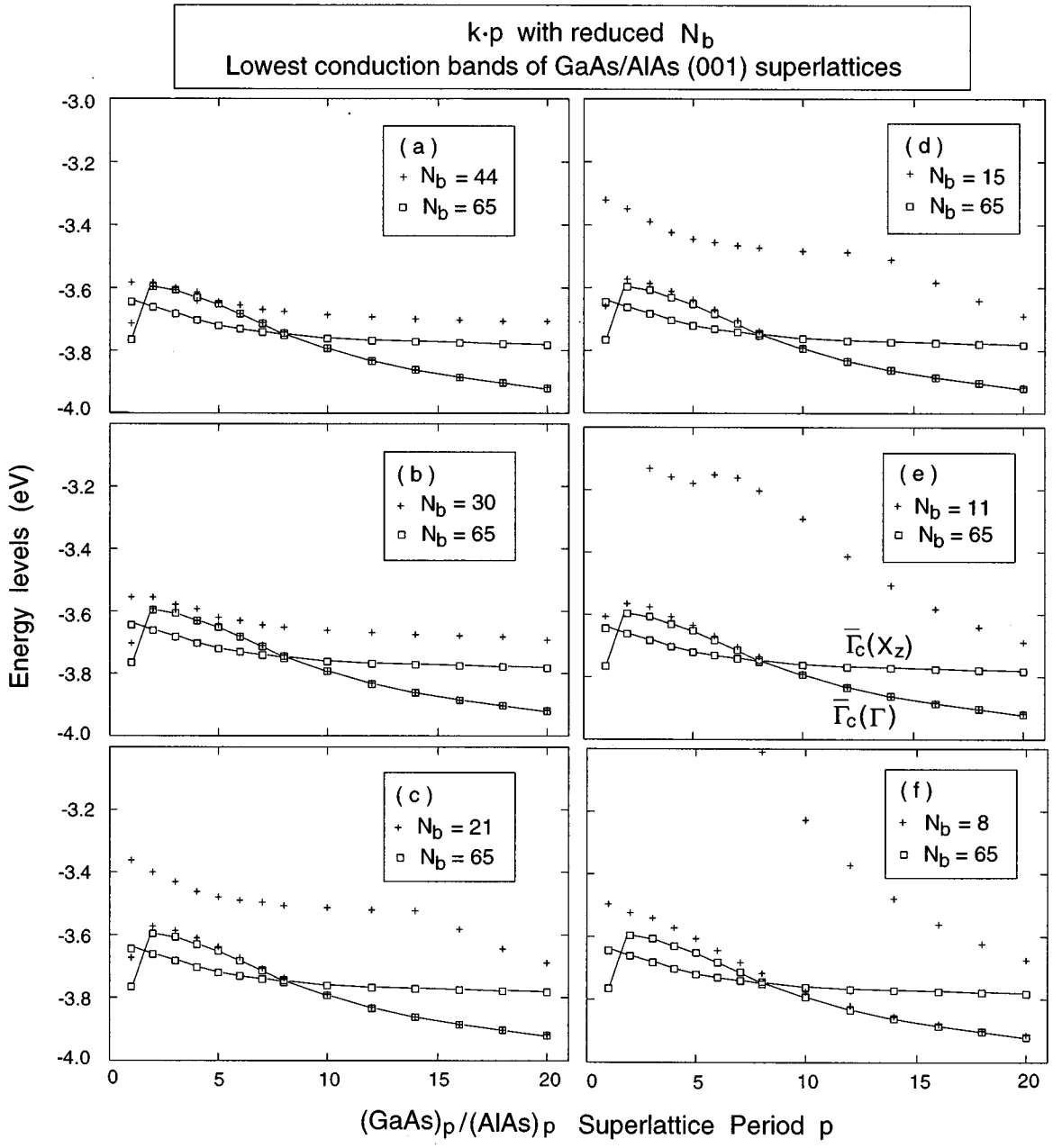

FIG. 7. Effects of reducing N_b on the energies of **k·p** GaAs/AlAs (001) superlattice conduction bands. An abrupt $w(r)$ is used and the $S^{A(B)}(n,m,k)$ is calculated directly from Eq. (18) for a primary set of **k** points and then interpolation for the other **k** points. $\tilde{U}(n,m)=\delta_{n,m}$ and $N_m=369$ are used in all calculations. The squares are the same results as the squares in Fig. 6(a).

both, so as to avoid double counting. To ensure that both choices yield the same result and, more importantly, that the $k=-k_X$ point (when $-X$ is chosen) couples properly with the $k=k_X-2\pi/L$ points (where L is the length of the system), we need $u^A_{n,-X}$ to behave like $u^A_{n,X}\exp(i2k_Xr)$. More precisely, we need to have

$$u^A_{n,-G/2}(r)=e^{i\theta_n}u^A_{n,G/2}(r)e^{i\mathbf{G}\cdot\mathbf{r}}. \tag{29}$$

This is the periodic condition of Bloch states between $k=-G/2$ and $k=G/2$. Here $e^{i\theta_n}$ is an arbitrary phase factor. Let $U^A(n,m,k)$ be an unitary transformation that diagonalizes the matrix $H^A(n,m,k)$ of Eq. (26). In the **k·p** formalism, we then have $u^A_{n,k}=\Sigma_{p=1}^{N_b}U^A(p,n,k)u^A_p$. Substituting this into Eq. (29) gives

$$\sum_{p=1}^{N_b}U^A(p,n,-G/2)u^A_p(r)$$
$$=e^{i\theta_n}\sum_{p=1}^{N_b}U^A(p,n,G/2)u^A_p(r)e^{i\mathbf{G}\cdot\mathbf{r}}. \tag{30}$$

Multiplying both sides by $u^{A*}_m(r)$, integrating over a primary cell, and using Eq. (28), we have

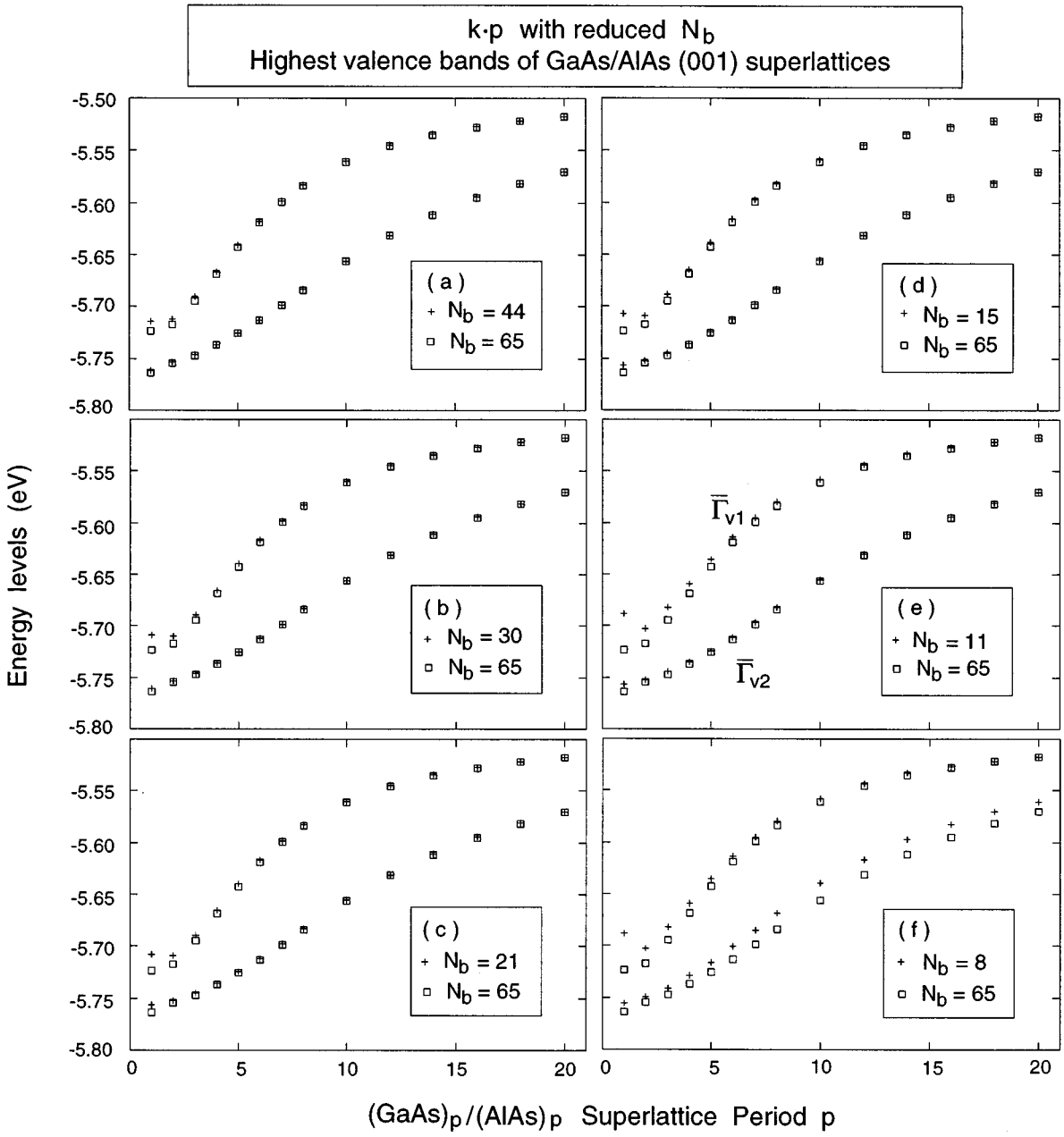

FIG. 8. Effects of reducing N_b on the **k·p** GaAs/AlAs (001) superlattice valence bands. The calculation conditions are the same as in Fig. 7. The squares are the same as the squares in Fig. 6(b).

$$U^A(n,m,-G/2)=e^{i\theta_m}\sum_{p=1}^{N_b} U^A(p,m,G/2)\mathcal{O}^A(p,n,-G). \tag{31}$$

This equation is automatically satisfied for $N_b=\infty$, but is no longer exactly true for a finite N_b. To satisfy it for $G/2=k_X$ and for $G/2=k_L$, we need to modify $\mathcal{O}^{A(B)}(n,m,2k_X)$ and $\mathcal{O}^{A(B)}(n,m,2k_L)$ from their original values given by Eq. (28). This modification is described in Appendix B. For $\mathcal{O}^{A(B)}(n,m,G)$ evaluated at other **G**'s, the direct result of Eq. (28) could be used in Eq. (27) without any change.

Once $\tilde{U}(n,m)$ and $\mathcal{O}^{A(B)}(n,m,G)$ are obtained, the Hamiltonian matrix $H_A^{\rm NS}(mk',mk)$ can be readily calculated from Eq. (24). However, because the approximations are made in conjunction with the finite N_b, the $H_A^{\rm NS}(mk',mk)$ calculated from Eqs. (24), (23), (20), and (17) is not exactly Hermitian. This non-Hermitian error can be measured by

$$\alpha=\sum_{mk',nk}|H_A^{\rm NS}(mk',nk)-H_A^{\rm NS*}(nk,mk')|\Big/\sum_{mk',nk}|H_A^{\rm NS}(mk',nk)|. \tag{32}$$

We find that α is of the order of 0.5×10^{-3} for our GaAs/AlAs systems. [Had we used $\tilde{U}(n,m)=\delta_{n,m}$, this α would be ten times larger.] To circumvent this non-

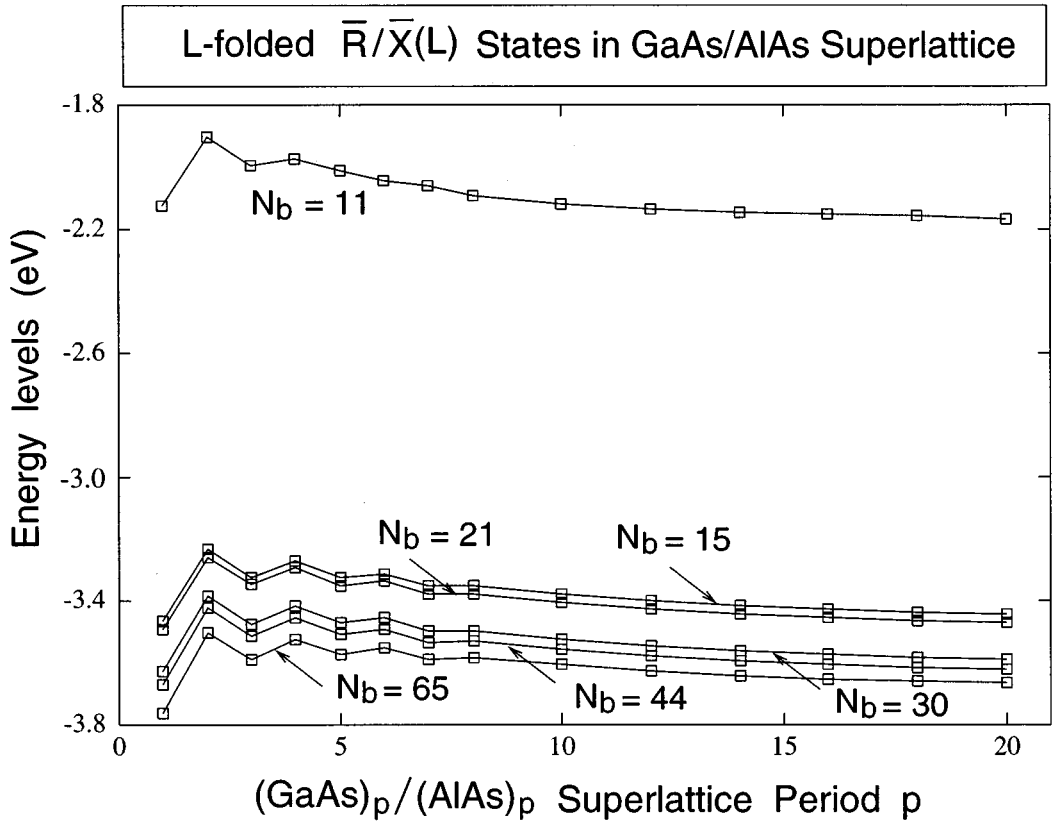

FIG. 9. Effects of reducing N_b on the **k·p** GaAs/AlAs (001) superlattice $\overline{R/X}(L)$ conduction bands. The calculation conditions are the same as in Fig. 7.

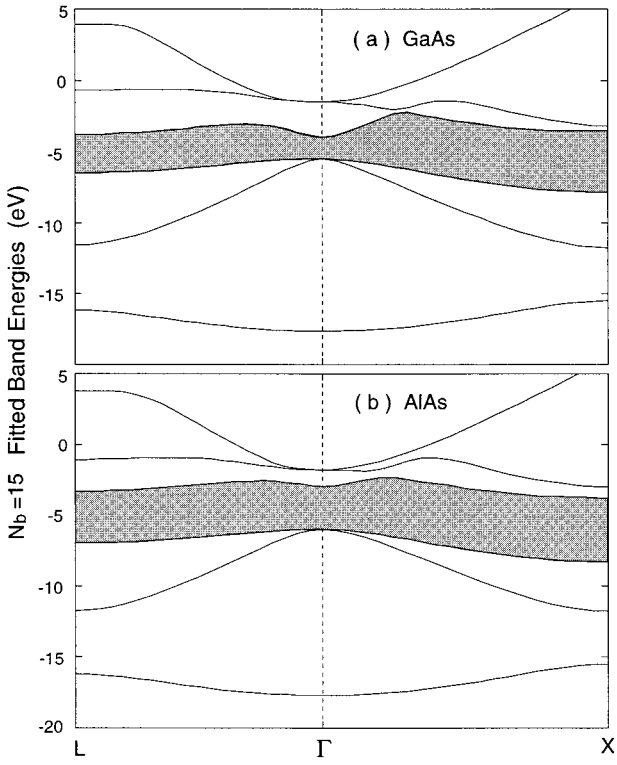

FIG. 10. Fitted **k·p** band structures of (a) bulk GaAs and (b) AlAs using $N_b=15$.

Hermitian problem, we simply symmetrize the matrix as $[H_A^{\rm NS}(mk',nk)+H_A^{\rm NS*}(nk,mk')]/2$ and then diagonalize the symmetrized matrix.

D. Choice of the interfacial potential

In Sec. IV C, the calculation of $S^{A(B)}(n,m,k)$ required a smooth $w(r)$ function [with zero $W(k)$ outside 2BZ]. However, in reality, the interface could be sharper than $V_w^{\rm NS}(r)$ calculated from such $w(r)$ via Eq. (10). Here we will introduce an interfacial potential to restore the sharpness of the interface from $V_w^{\rm NS}(r)$:

$$V^{\rm IF}(r)=V_{\rm sharp}^{\rm NS}(r)-V_w^{\rm NS}(r), \tag{33}$$

where the superscript IF stands for interface.

$V^{\rm IF}(r)$ defined in Eq. (33) is localized at the interface and is the interfacial potential for the whole system. We first break it down to its constituents belonging to each primary cell of the interface. Let us first define an interface primary cell of $A(B)$ as a primary cell for material $A(B)$ that has at least one $B(A)$ neighboring primary cell. We will use $\mathcal{R}$ to denote one interfacial primary cell and its position and $A/I(B/I)$ to denote the domain of the interfacial primary cell. To break down $V^{\rm IF}(r)$, we have

$$V^{\rm IF}(r)=\sum_{\mathcal{R}\in A/I} V^A(r-\mathcal{R},\mathcal{R})+\sum_{\mathcal{R}\in B/I} V^B(r-\mathcal{R},\mathcal{R}), \tag{34}$$

where $V^{A(B)}(r,\mathcal{R})$ is the interfacial potential contribution from interfacial primary cell $\mathcal{R}$. It should only depend on the

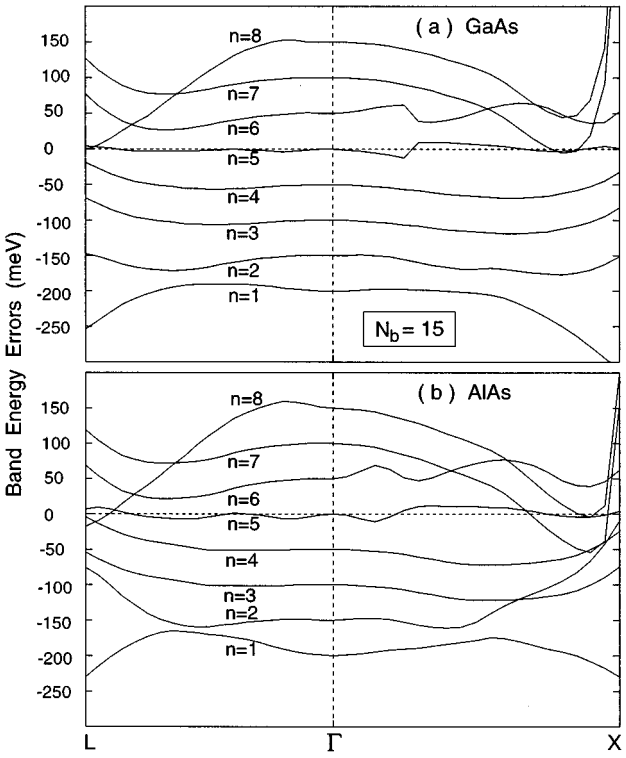

FIG. 11. Errors $\epsilon_{\mathbf{k}\cdot\mathbf{p}}-\epsilon_{\mathrm{PWP}}$ in band energies of the fitted ($N_b=15$) $\mathbf{k}\cdot\mathbf{p}$ band structures of Fig. 10 for (a) bulk GaAs and (b) AlAs compared with the direct PWP results. The curves for different bands are shifted for clarity (they should all be zeros at the Γ point). These errors are much smaller than the unfitted errors of $N_b=15$ shown in Fig. 4.

local atomic arrangements surrounding $\mathcal{R}$. We will further break down $V^A(r,\mathcal{R})$ into its contribution from the neighboring B-type primary cells. Suppose that an A-type primary cell $\mathcal{R}$ has $m(\mathcal{R})$ neighboring primary cells of type B; then

$$V^A(r,\mathcal{R})=\sum_i^{m(\mathcal{R})} V^A_{\gamma_i}(r), \tag{35}$$

where the subscript γ_i indicates the position of the neighboring primary cell. Considering only the nearest neighbors of a fcc primary cell of the zinc-blende lattice, we have 12 possible position γ_i. Their $V^A_{\gamma_i}(r)$ are connected by symmetry operations so only one of them needs to be studied here [say, $\gamma_i=xy$, the neighboring position of $(110)a/2$].

Suppose the matrix element of $V^A_{\gamma_i}(r)$ in the A-type Γ Bloch basis is

$$H^A_{\gamma_i}(m,n,k)\equiv\int u^{A*}_m(r)V^A_{\gamma_i}(r)u^A_n(r)e^{-i\mathbf{k}\cdot\mathbf{r}}d^3r; \tag{36}$$

then the Hamiltonian matrix of $V^{\mathrm{IF}}(r)$ under this basis is

$$\begin{aligned}H^{\mathrm{IF}}_A(mk',nk)&\equiv\frac{1}{N_c}\langle u^A_m e^{i\mathbf{k}'\cdot\mathbf{r}}|V^{\mathrm{IF}}(r)|u^A_n e^{i\mathbf{k}\cdot\mathbf{r}}\rangle\\&=\sum_{\mathcal{R}\in A/I}\sum_{i=1}^{m(\mathcal{R})}H^A_{\gamma_i}(m,n,k'-k)\frac{1}{N_c}e^{-i(k'-k)\mathcal{R}}\\&\quad+\sum_{\mathcal{R}\in B/I}\sum_{i=1}^{m(\mathcal{R})}H^{B'}_{\gamma_i}(m,n,k'-k)\\&\quad\times\frac{1}{N_c}e^{-i(k'-k)\mathcal{R}}.\end{aligned} \tag{37}$$

Here $H^{B'}_{\gamma_i}$ is $H^B_{\gamma_i}$ in the u^A_n basis (instead of the u^B_n basis); thus

$$H^{B'}_{\gamma_i}(n,m,k)=\sum_{p,p'=1}^{N_b}\tilde{U}^*(p,n)H^B_{\gamma_i}(p,p',k)\tilde{U}(p',m). \tag{38}$$

Finally, after adding the interfacial potential term, the total Hamiltonian matrix is

$$H^{\mathrm{tot}}_A(mk',nk)=H^{\mathrm{NS}}_A(mk',nk)+H^{\mathrm{IF}}_A(mk',nk). \tag{39}$$

This $H^{\mathrm{tot}}_A(mk',nk)$ will be diagonalized to get the nanostructure eigenenergies.

In the above formalism, a different choice of $V^{A(B)}_{\gamma_i}(r)$ corresponds to a different choice of interfaces. In Appendix C,[31] we have chosen a very simple model to describe $V^{A(B)}_{\gamma_i}(r)$ [in conjunction with a description of $W(r)$]. To determine the interfacial potential, we have adjusted the parameters in this simple model, so that our $\mathbf{k}\cdot\mathbf{p}$ results of this V^{IF} agree with the direct plane-wave diagonalization results of a pseudopotential interface model.[31]

TABLE I. Fitted mass parameters and coefficients $a^{A(B)}_n$ of the $f(k)$ terms in Eq. (26). The unit of mass parameters is electron mass and the unit of $a^{A(B)}_n$ is hartree bohrs^4. The parameters are the same for the partners of a degenerate set.

Band index n	m_n(GaAs)	m_n(AlAs)	a_n(GaAs)	a_n(AlAs)
1	1.0089	1.0015	-0.0035	0.0108
2,3,4	1.0509	1.0665	0.0055	-0.0110
5	1.1074	1.1713	-0.0038	0.0695
6,7,8	1.0593	1.0793	0.0095	0.0511
9,10	1.0145	1.0003	0.0096	0.0103
11	1.1964	1.4057	0.0239	0.0267
12,13,14	1.1370	1.1297	0.0298	-0.0115
15	1.0855	1.1668	0.0095	0.0050

E. Summary of practical equations

In summary, in order to solve the generalized multiband $\mathbf{k}\cdot\mathbf{p}$ problem [Eqs. (24) and (39)] for a system of interest, the following inputs are needed: (i) $H^{A(B)}(n,m,k)$ of Eq. (26), which require $\epsilon^{A(B)}_{n,0}$ $m^{A(B)}_n$ $a^{A(B)}_n$, and $P^{A(B)}(n,m)$. (ii) $\mathcal{O}^{A(B)}(n,m,G)$ of Eq. (27) for a few special $\mathbf{G}$ points ($G=\Gamma,2X,\ldots$), (iii) $\tilde{U}(n,m)$ of Eq. (23); (iv) $W(k)$ of Eqs. (27) and (C6), which requires α_1, α_2, and k_c; and (v) the interfacial potential $a^{A(B)}_{xy}(n)$ of Eq. (C5), which requires $a_1,\ldots,a_5$, $f_L(n)$, and $f_X(n)$. These input parameters for GaAs and AlAs are listed in Tables I and II and the matrices are stored in a file transfer protocol (FTP) site.[32] The key equations to be used to solve a general nanostructure problem are Eqs. (17), (23), (24), (26), (27), (37)–(41), (C2), and (C4)–(C7).

TABLE II. Interfacial parameters $\{a_i\}$ of Eq. (C5) in eV and α_1, α_2, and k_c of Eqs. (C6) and (C7) in a.u.

a_1	a_2	a_3	a_4	a_5	α_1	α_2	k_c
-0.001	-0.018	0.030	-0.087	0.270	2.263	-0.510	0.567

V. RESULTS FOR NANOSTRUCTURES USING THE MULTIBAND k·p METHOD

A. Superlattices in the u_0 represenation

The comparisons between the multiband **k·p** and the direct plane-wave diagonalization results for the superlattice energy levels are shown in Figs. 12 and 13. As we can see, the trends in the results of the direct diagonalization and the multiband **k·p** are similar. The even-odd oscillations in the multiband **k·p** results are apparent; the oscillation amplitudes are in fact close to those obtained in the plane-wave calculations. These oscillations are missed in previous standard **k·p** calculations.[16] The only large difference between the multiband **k·p** and the plane-wave results occurs at the monolayer limit $p=1$, at which our model for the interfacial terms breaks down. For all other p's, the largest error is about 15 meV. On average, the error is much smaller. For $p \lesssim 10$ the average error is ~ 5 meV, while for larger p, the average error is about 2–3 meV (close to the bulk band-structure error). Overall, the multiband **k·p** performs very well. This can be contrasted with the standard **k·p** model,[16] where (i) some of the superlattice states are completely missed, (ii) some of the trends in the energy vs period curves are very different from the plane-wave results, and (iii) there are no even-odd oscillations.

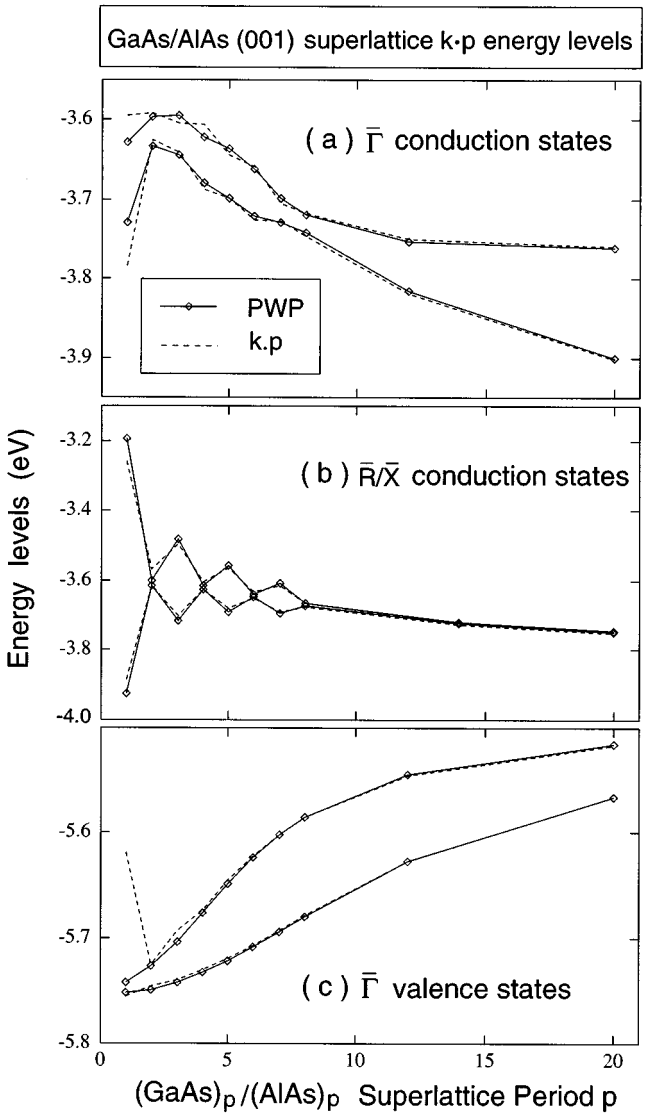

FIG. 12. GaAs/AlAs (001) superlattice multiband **k·p** energy levels (dashed lines) compared with the results of direct PWP calculation (solid lines and diamonds).

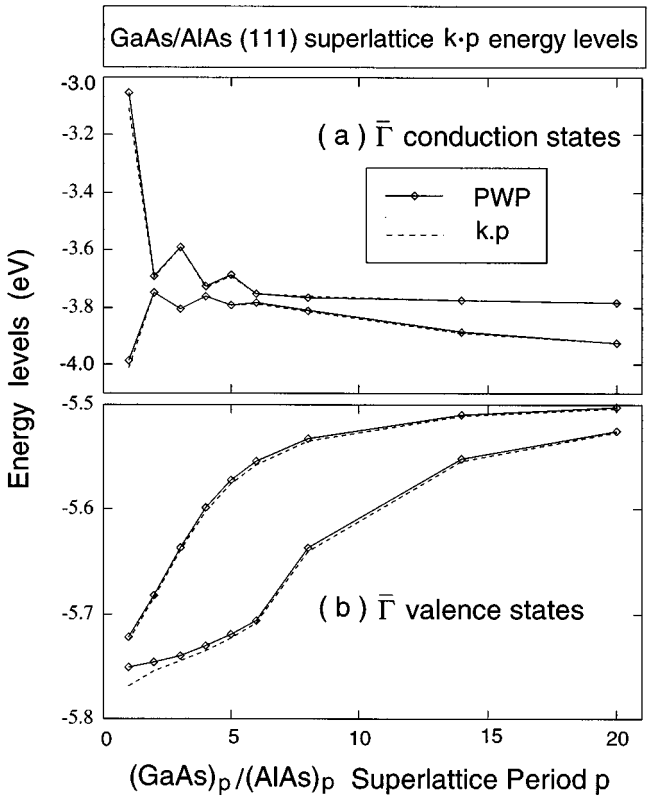

FIG. 13. GaAs/AlAs (111) superlattice multiband **k·p** energy levels (dashed lines) compared with the results of direct PWP calculation (solid lines and diamonds).

B. Superlattice with reduced k points and in the u_k representation

In Sec. IV we treated $H_A^{\rm tot}(mk',nk)$ [Eq. (39)] in the u_0 representation, retaining all **k** points. However, for three-dimensional nanostructures (e.g., quantum dots), this matrix could be too large for direct diagonalization. We will next test methods that reduce the number of **k** points and the number of bands in the basis-set expansion. After all, this is the reason we use the **k·p** formalism: as discussed in the Introduction, the basis set can be drastically reduced for large systems compared with the plane-wave calculations.

One advantage of using the basis of Eq. (12) is that for very large systems, the sum over **k** can be restricted. This is so because the larger the system, the smoother the envelope function of $u_n(r)$, so we can use a fixed number of Fourier

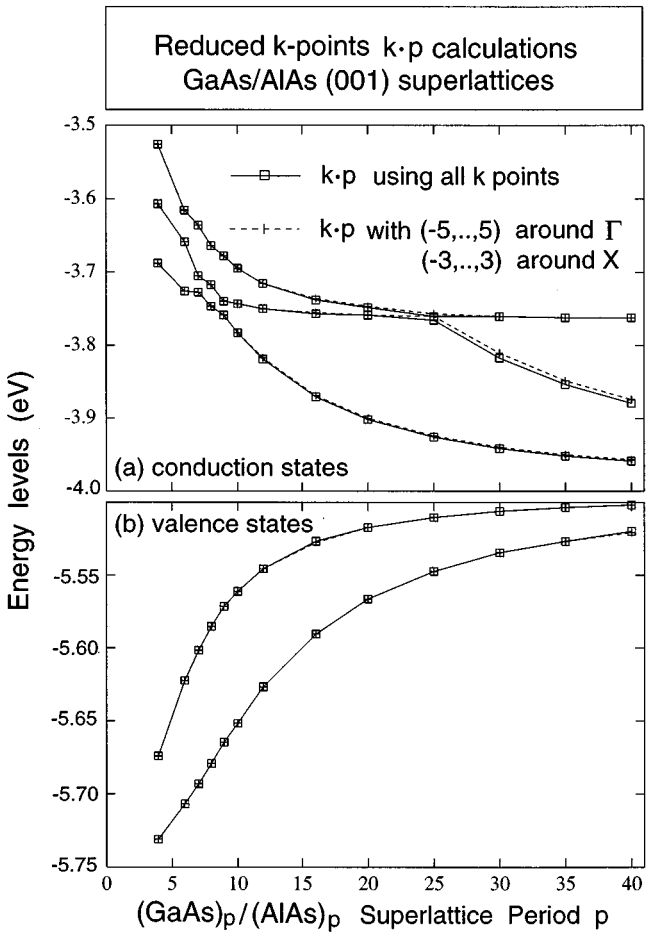

FIG. 14. Reduced **k**-point multiband **k·p** GaAs/AlAs (001) superlattice energy levels (dashed lines and pluses) compared with the full **k**-point multiband **k·p** results (solid lines and squares).

components in Eq. (1) or (12). In practice, we will select a fixed number of **k** points around the bottom of the physically interesting band-structure valleys (e.g., Γ, X, and L), regardless of the size of the nanostructure.

In Fig. 14 we show the results for the (001) $(\mathrm{GaAs})_p/(\mathrm{AlAs})_p$ superlattices using a fixed number of **k** points in the basis set of Eq. (12). As can be seen, if we have $\Delta k=(-5,\ldots,0,\ldots,5)(2\pi/L)$ (where L is the length of the supercell) around Γ (i.e., $k=k_\Gamma+\Delta k$) and $\Delta k=(-3,\ldots,0,\ldots,3)(2\pi/L)$ around X, then the fixed **k**-point basis introduces an error of only 3 meV for the band-edge Γ- and X-folded states. Thus, in a three-dimensional (quantum dot) calculation, we could use the $(-5,\ldots,5)$ and $(-3,\ldots,3)$ as the cutoff spherical diameters around Γ and X to select **k** points in the basis. A similar diameter exists for the L point. Using these diameters, we need typically only 1000–2000 **k** points for a three-dimensional system.

We next reduce the number of bands in the basis. As shown in Fig. 7, reducing the number of band in the $u_{n,\Gamma}$ basis will introduce large errors. The most effective approach is to first change the Hamiltonian matrix from the $\{u_{n,\Gamma}\}$ basis [Eq. (12)] to the $\{u_{nk}\}$ basis [Eq. (13)] and *then* reduce the number of bands in the $\{u_{nk}\}$ basis. Projection analysis[16] tells us that the nanostructure eigenstates consist mostly of only a few u_{nk} bands n. Thus, using the $\{u_{nk}(r)\}$ basis, we can dramatically reduce the number of states n at each **k** point.

When we change the basis from the u_0 representation to the u_k representation, we also have a choice of using u^A_{nk} or u^B_{nk} or using a *mixture* of u^A_{nk} *and* u^B_{nk} [in the u_0 representation, using u^A_n or u^B_n for all the 15 bands will give the same results; see Eqs. (23) and (24) and Appendix B]. Within the **k·p** formalism, this general basis u^α_{nk} can always be represented by the Γ-point basis set $\{u^A_n\}$:

$$u^\alpha_{nk}=\sum_{m=1}^{N_b} U^\alpha(m,n,k)u^A_m. \tag{40}$$

$U^\alpha(m,n,k)$ can be obtained for each **k** independently, so computationally, this is not very demanding. Getting $U^\alpha(m,n,k)$ involves a diagonalization of $H^{A(B)}(m,n,k)$ of Eq. (26) and the use of the unitary transformation matrix $\tilde{U}(m,n)$, which connects u^B_n with u^A_n. If some states of both u^A_{nk} and u^B_{nk} are used for a same **k**, then orthogonalization among them is necessary, so that the resulting $U^\alpha(m,n,k)$ is orthonormal among different n's. Once $U^\alpha(m,n,k)$ is obtained, the Hamiltonian matrix under the new basis set u^α_{nk} is

$$H^{\mathrm{tot}}_\alpha(mk',nk)=\sum_{p,p'=1}^{N_b} U^{\alpha *}(p',m,k')H^{\mathrm{tot}}_A(p'k',pk) \times U^\alpha(p,n,k). \tag{41}$$

Note that the number of bands (m,n) in $H^{\mathrm{tot}}_\alpha(mk',nk)$ could be much smaller than $N_b=15$. Thus $H^{\mathrm{tot}}_\alpha(mk',nk)$ can be diagonalized directly for three-dimensional systems.

To test the accuracy of the various reduced basis sets $\{u^\alpha_{nk}\}$ in our multiband **k·p** method, we show in Fig. 15 a comparison between results using all the 15 u_{nk} bands and a reduced number of u_{nk} bands. For the Γ- and X-folded lowest conduction bands, we illustrate the results using (a) six lowest bands of GaAs plus the fifth band of AlAs, (b) the five lowest bands of GaAs plus the fifth band of AlAs, and (c) the fifth band of GaAs for **k** points around Γ and the fifth band of AlAs for **k** points around X (so there is only one state for each **k** point). From Fig. 15 we see that the (a) and (b) basis sets are quite accurate, with small errors for long superlattices and $\sim$ 7 meV error for short superlattices. The single band basis (c) is not as accurate as (a) and (b) for short period superlattices. However, for long superlattices, it is still very good. Since our method is aimed primarily at large nanostructures, such as long period superlattices, and since the number of basis functions in set (c) is 6–7 times smaller than in set (a) or (b), we will use set (c) in our following calculations of large, three-dimensional quantum dots.

A hybrid approach of the u_0 and u_k representation was recently developed by Froyen.[33] There the Hamiltonian matrix elements under the hybrid basis function are directly evaluated for a few $\{k,k'\}$ points. The matrix elements of other $\{k,k'\}$ points are interpolated using the **k**-space power expansions around these directly calculated $\{k,k'\}$ points.

C. Embedded GaAs quantum dots: A 250 000-atom problem

We now apply the current method to study a Ga-centered spherical GaAs quantum dot embedded in an AlAs matrix. We would like to determine the dot size beyond which the conduction-band minimum reverts from the X_{1c}(AlAs) state

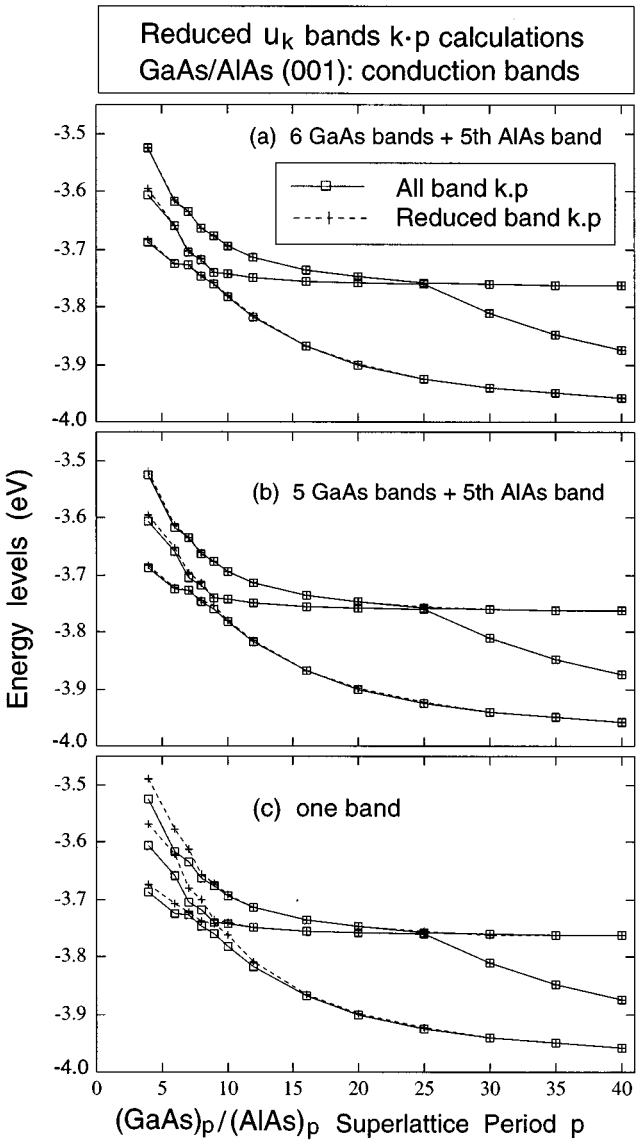

FIG. 15. Reduced band **k·p** GaAs/AlAs (001) superlattice conduction-band energy levels (dashed lines and pluses) compared with the all band **k·p** results (solid lines and squares). The one-band calculation in (c) uses the fifth GaAs state for **k** points close to Γ and the fifth AlAs state for **k** points close to *X*.

to the Γ_{1c}(GaAs) state.[23] At the (anti)crossing point, there could be a Γ-*X* coupling. The computational difficulty of this problem is that in a supercell description, very thick AlAs barriers are needed to avoid overlap of neighboring GaAs quantum-dot wave functions.[23] We have calculated GaAs quantum dots up to 160 Å in diameter, while the size of AlAs matrix is kept at $50\times50\times50$ primary cells. This corresponds to a 250 000 atoms.

The $C^{A(B)}(k)$ structure factor defined in Eq. (19) and its counterparts for the interfacial potentials in Eq. (37) were calculated using fast Fourier transforms. **k**-point selection spheres are placed at the Γ point and the three *X* points using slightly larger diameters of $(-6,\ldots,0,\ldots,6)$ and $(-4,\ldots,0,\ldots,4)$ than the ones used in Fig. 14. There are 2260 **k** points in total. When the selected **k** point is inside the sphere of the Γ point, $u_{5,k}^{\mathrm{GaAs}}$ is used in the basis set. When the selected **k** point is inside the spheres of the *X* point, $u_{5,k}^{\mathrm{AlAs}}$ is used in the basis set. So, the total number of basis function is also 2260. The total CPU time for calculating the matrix $H_{\alpha}^{\mathrm{tot}}(mk',nk)$ and diagonalizing it is less than 30 min on an IBM/6000 workstation model 590. The calculation takes about 100 megabyte memory, mainly to host the 2260×2260 double precision complex matrix $H_{\alpha}^{\mathrm{tot}}(mk',nk)$.[34]

The results are shown in Fig. 16. The crossover diameter between type-I and type-II behavior is found to be 70 Å. However, surprisingly, we find no coupling between the Γ- and *X*-induced states. Due to the spherical shape of the quantum dot, the three *X*-point states are degenerated. They have a different symmetry representation than the single degenerated Γ state. Thus the Γ and *X* states do not couple in this case. To get a Γ-*X* coupling, some other shapes (e.g., disk) of the quantum dot, or a spherical dot with an As atom at its origin, is needed. In addition, pressure-dependent rather than size-dependent eigenenergy curves might be needed to find small Γ-*X* anticrossing since smooth curves are available only in the pressure-dependent case.

VI. COMPARISON WITH OTHER METHODS

In this section we summarize briefly the similarities and differences of the current method with alternative approaches.

A. Comparison with the standard k·p model

Formally, our method differs from the standard **k·p** model by the use of a u_0 basis of pure *A* [Eq. (12)] leading to the appearance of an overlap matrix $S^A(n,m,k)$ [Eq. (18)] in the evaluation of the Hamiltonian matrix in Eq. (17). Besides, due to the use of many bands, our wave vector **k** is restricted to reside inside the BZ. Thus, unlike the standard **k·p** model, our Hamiltonian equation cannot be formally changed to a differential equation.

Practically, we include many-band (15 for GaAs/AlAs) rather than four-band coupling and a bulk band structure that is accurate over the *entire* BZ. As a result, we are able to reproduce the energetic features of short period superlattices (Figs. 12 and 13) missed by the standard model.[16]

B. Comparison with direct plane wave diagonalization

In the direct plane-wave diagonalization [Eqs. (2) and (3)], the basis functions are classified according to momentum alone, not band index, so there is no intuitive way to select the variationally most important states. Instead, one has to increase systematically the basis size. In contrast, in the u_0 representation, and more so in the u_k representation, one can preselect basis functions on the basis of their likely coupling in the nanostructure band edge states. This is decided based on the proximity of the energy of a given bulk basis function to the band edges.

We have recently developed the ''folded spectrum method'' (FSM) (Ref. 14) to efficiently solve for the band-gap edge states of nanostructures. The FSM provides exact solutions of the plane-wave diagonalization, so the FSM solutions are superior to the current **k·p** approach (if the current **k·p** Hamiltonian is developed from the plane-wave pseudopotential Hamiltonian). The problem with the FSM is that when the system is much larger than a few thousand

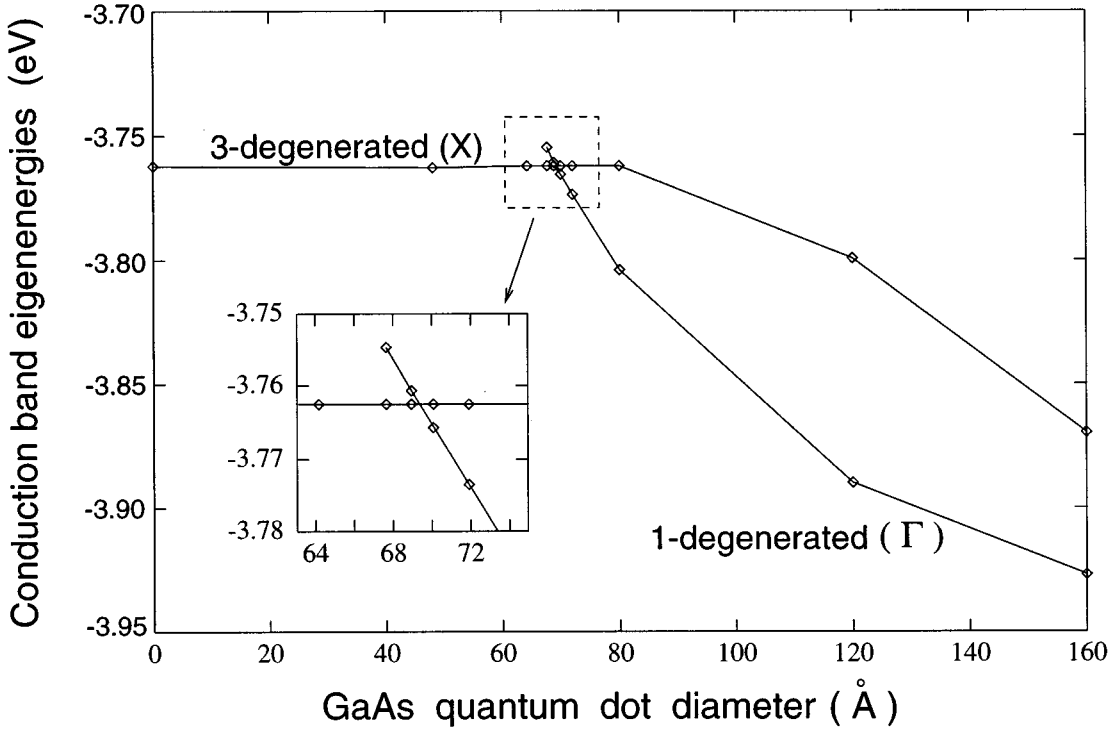

FIG. 16. Lowest conduction-band energy levels of spherical GaAs quantum dots embedded in AlAs matrix vs dot size. The inset shows the Γ-X crossing.

atoms, the FSM is too time consuming. In such cases, the current $\mathbf{k}\cdot\mathbf{p}$ method can be used as a substitute. The FSM is well suited to solve for random alloys,[35] rough interfaces,[36] and isolated quantum dots.[14,22] In cases of three-dimensional nanostructures with shallow barriers (e.g., material A embedded in material B quantum dots), usually larger systems ($>10\,000$ atoms) are needed. The current method is designed to solve just such problems.

ACKNOWLEDGMENTS

The authors would like to thank Dr. A. Franceschetti, Dr. S. Froyen, and Dr. D. Wood for many helpful discussions. This work was supported by the office of Energy Research, Material Science Division, U.S. Department of Energy, under Grant No. DE-AC02-83CH10093.

APPENDIX A: CREATING A PLANE-WAVE BASIS FROM A POLYHEDRON

In the conventional plane wave basis calculation of Eqs. (2) and (3), a sphere of radius $G_{\rm cut}=\sqrt{2E_{\rm cut}}$ (where $E_{\rm cut}=6.5$ Ry) is used to select the plane-wave basis $\{G\}$. This sphere contains 65 plane-wave functions at the $k=\Gamma$ point. When the $\mathbf{k}$ point moves away from Γ, the number of plane-wave basis functions enclosed within the $\mathbf{k}$-centered radius-$G_{\rm cut}$ sphere may also change. The $\mathbf{k}\cdot\mathbf{p}$ formalism with $N_b=65$ cannot reproduce this change of the plane-wave basis set. As a result, there is a 20 meV energy difference between the $N_b=65$ $\mathbf{k}\cdot\mathbf{p}$ results and the plane-wave calculations at the X and L points. (Using a smooth $E_{\rm cut}$ technique described in Ref. 26, the band structure of the plane-wave calculation is smooth, despite the possible sudden change of the number of the plane-wave functions.) We need to eliminate this difference, so that we can produce an exact $\mathbf{k}\cdot\mathbf{p}$ result that could be compared with the results of the direct plane-wave diagonalization. To this end, instead of using a conventional $G_{\rm cut}$-radius sphere centered at the $\mathbf{k}$ point, we will use a special polyhedron zone to select the plane-wave basis. This zone is also centered at the $\mathbf{k}$ point when $\mathbf{k}$ is away from Γ. It has a shape of Wigner-Seitz primitive cell of the *real-space* crystal lattice. Thus, its surfaces are parallel to the planes of the reciprocal lattice. When $k=\Gamma$, these surfaces are in the middle of two neighboring parallel reciprocal-lattice planes. The advantage of this special polyhedron zone is that when $\mathbf{k}$ moves within the first BZ, this polyhedron will not cut through any reciprocal lattice points, thus the plane-wave basis will not be changed. Consequently, the $N_b=65$ $\mathbf{k}\cdot\mathbf{p}$ band structure is exactly the same as obtained in direct plane-wave diagonalization. This zone is used only in Sec. III.

APPENDIX B: THE CORRECTION OF $\widetilde{U}(n,m)$ AND $O_A(n,m,G)$

In the following, we discuss separately the correction of $\widetilde{U}(n,m)$ and the correction of $\mathcal{O}_A(n,m,G)$.

When $N_b=15$, the $\widetilde{U}(n,m)$ defined in Eq. (22) is no longer unitary. The following procedure will be used to make it unitary. Assume that $\widetilde{U}'(n,m)$ is the original result calculated from Eq. (22). Define

$$M(n,m)=\sum_{p=1}^{N_b}\widetilde{U}'^{*}(p,n)\widetilde{U}'(p,m). \tag{B1}$$

Because $M(n,m)$ is positive definite, we can compute the quantity $M^{-1/2}(n,m)$. Then, the unitary matrix $\widetilde{U}(n,m)$ to be used in Eq. (23) is

$$\widetilde{U}(n,m)=\sum_{p=1}^{N_b}\widetilde{U}'(n,p)M^{-1/2}(p,m). \tag{B2}$$

Equation (31) needs to be satisfied by $\mathcal{O}^A(p,n,G)$. But for $N_b=15$, this equation is usually not satisfied by $\mathcal{O}^A(p,n,G)$ calculated from Eq. (28). To make it so, the following procedure is used. Let $\mathcal{O}^{A'}(n,m,G)$ denote the original matrix calculated by Eq. (28). We then construct $I^{A'}$ as

$$I^{A'}(n,m,G)=\sum_{p,p'=1}^{N_b}U^A(p,n,-G/2)\mathcal{O}^{A'}(p,p',G)\times U^{A}*(p',m,G/2). \tag{B3}$$

If $\mathcal{O}^{A'}$ satisfies Eq. (31), then $I^{A'}$ should equal $\delta_{n,m}e^{-i\theta_n}$. For $N_b=15$, this is not the case. For our GaAs and AlAs systems, we found that for the first six bands of $G=2k_X$ and the first eight bands of $G=2k_L$, the corresponding subspace of $I^{A'}$ is very close to $\delta_{n,m}e^{-i\theta_n}$ (with the amplitude of the diagonal elements to be >0.95). But for higher-energy bands, the amplitude of the diagonal elements in $I^{A'}$ is very small. So, to satisfy Eq. (31) for the most important bands n (the first six for $G=2k_X$ and the first eight for $G=2k_L$) and without changing $I^{A'}$ too much, we have modified $I^{A'}(n,m,G)$ to $I^A(n,m,G)$ as

$$I^A(n,m,G)=\begin{cases}\dfrac{I^{A'}(n,n,G)}{|I^{A'}(n,n,G)|}\delta_{n,m} & \text{if } n \text{ or } m<6(\text{or } 8)\\ I^{A'}(n,m,G), & \text{otherwise.}\end{cases} \tag{B4}$$

After this step, $\mathcal{O}^A(n,m,G)$ is calculated as

$$\mathcal{O}^A(n,m,G)=\sum_{p,p'=1}^{N_b}U^A*(n,p,-G/2)I^A(p,p',G)\times U^A(m,p',G/2). \tag{B5}$$

This $\mathcal{O}^A$ satisfies Eq. (31) for the most important bands and is also close to the $\mathcal{O}^{A'}$ calculated from Eq. (28). Special care must be exercised for degenerated bands in Eq. (31). In practice, we have taken a k slightly off the X or L points, so that the exact degeneracy is lifted.

APPENDIX C: MODELING THE $V^A_{\gamma_i}(r)$ POTENTIAL

Here we use simple models to approximate $V^A_{\gamma_i}(r)$ and $H^A_{\gamma_i}(m,n,k)$. Because of the symmetry, it is suffice to discuss one γ_i direction, say, $\gamma_i=xy$. We would first like to control the spatial width of $V^A_{xy}(r)$ by $w(r)$ in Eq. (10); thus

$$V^A_{xy}(r)=v^A_{xy}(r)w(r), \tag{C1}$$

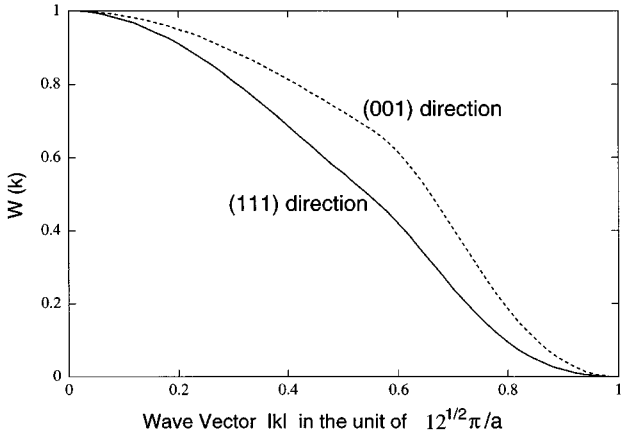

FIG. 17. Fourier components of $w(r)$ in the (001) and (111) directions.

where $v^A_{xy}(r+R)=v^A_{xy}(r)$ is a periodic function of crystal lattice R. It is easy to prove that the H^A_{xy} defined in Eq. (36) is

$$H^A_{xy}(m,n,k)=\sum_{p=1}^{N_b}[h^A_{xy}(p,n)S^A(p,m,k)+S^A(n,p,k)h^A_{xy}(m,p)]/2, \tag{C2}$$

where

$$h^A_{xy}(n,m)=\int_{\mathrm{PC}}u^{A}_n*(r)u^A_m(r)v^A_{xy}(r)d^3r. \tag{C3}$$

The merit of Eqs. (C1)–(C3) is that the **k** dependence of $H^A_{xy}(m,n,k)$ has been shifted to $S^A(m,n,k)$, which we already know [Eqs. (18) and (27)]. What remains is a **k**-independent matrix $h^A_{xy}(n,m)$, which we are going to describe. Using a very simple model, we will keep only the diagonal part of $h^A_{xy}(n,m)$; hence

$$h^A_{xy}(n,m)=a^A_{xy}(n)\,\delta_{n,m}. \tag{C4}$$

In our GaAs/AlAs system, we have the following expression for $a^{A(B)}_{xy}(n)$:

$$a^{\mathrm{GaAs}}_{xy}(n)=a_1\delta_{n,2}+a_1\delta_{n,3}+a_2\delta_{n,4}+a_3\delta_{n,5}+a_4f_L(n),$$

$$a^{\mathrm{AlAs}}_{xy}(n)=a_5f_X(n), \tag{C5}$$

where $n=2,3,4$ are the Γ-point top of the valence-band, p_x, p_y, and p_z states, respectively. $n=5$ is the bottom of conduction-band state. $f_L(n)\equiv|\langle u^{\mathrm{GaAs}}_{n\Gamma}|u^{\mathrm{GaAs}}_{5L}\rangle|^2$, except for $n<6$, where $f_L(n)\equiv 0$. $f_X(n)\equiv|\langle u^{\mathrm{AlAs}}_{n\Gamma}|u^{\mathrm{AlAs}}_{5X}\rangle|^2$, except for $n<6$, where $f_X(n)\equiv 0$. So we have five parameters to describe the interfacial potential: two parameters (a_1,a_2) are needed to describe its effects on the top of the GaAs valence bands at Γ, one (a_3) for its effects on the GaAs conduction-band minimum at Γ, one (a_4) for its effects on the lowest GaAs conduction band at L, and one (a_5) for its effects on the bottom of the AlAs conduction band at X.

Because the width of the interfacial potential is controlled by $w(r)$ through Eq. (C1), to get a sharp interface, it is also necessary to change $w(r)$. Note that $w(r)$ need not be a spherical function. Thus we can expressed $W(k)$ as a general function

$$W(k)=e^{-[k^2\alpha_1+f(k)/k^2\alpha_2]}F(|k|), \tag{C6}$$

where $f(k)=3(k_x^4+k_y^4+k_z^4)-k^4$, as defined in the text, and $F(|k|)$ is defined as

$$F(|k|)=\begin{cases}1 & \text{for } |k|<k_c\\ \frac{1}{2}+\frac{1}{2}\cos[(|k|-k_c)/(2\sqrt{3}/a-k_c/\pi)] & \text{for } k_c<|k|<2\sqrt{3}\pi/a\\ 0 & \text{for } |k|>2\sqrt{3}\pi/a.\end{cases} \tag{C7}$$

So there are three parameters α_1, α_2, and k_c to describe $W(k)$. $W(k)$ is nonzero only for $|k|$ within $2\sqrt{3}\pi/a$, where a is the fcc lattice constant. This means that only $\mathcal{O}^{A(B)}(n,m,G)$ for $G=2k_X,2k_L,(110)(2\pi/a)$ and their symmetric counterparts are needed as input matrices in Eq. (27). Further numerical tests show that ignoring $\mathcal{O}^{A(B)}(n,m,G)$ for $G=(110)(2\pi/a)$ only introduces a small error of $\sim$1–2 meV. Thus, we will ignore $\mathcal{O}^{A(B)}(n,m,G)$ at this **G** point, although including it is straightforward.

The different choices of the above parameters $\{a_n\}$ and α_1,α_2,k_c yield different choices of the interfaces. The final parameters are determined such that the resulting **k·p** eigenenergies of a few superlattices can be close to that of the direct plane-wave diagonalization calculations based on an atomic pseudopotential interface model.[31] The parameters $\{a_i\}$, α_1, α_2, and k_c are listed in Table II and $W(k)$ is shown in Fig. 17.

*Present address: Biosym/MSI, 9685 Scranton Road, San Diego, CA 92121.

[1] J.M. Luttinger and W. Kohn, Phys. Rev. **97**, 869 (1955).
[2] E.O. Kane, J. Phys. Chem. Solids. **1**, 249 (1957).
[3] M. Cardona and F.H. Pollak, Phys. Rev. **142**, 530 (1966).
[4] G. Bastard, J.A. Brum, and R. Ferreira, in *Solid State Physics*, edited by D. Turnbull and H. Ehrenreich (Academic, New York, 1991), Vol. 44, p. 229.
[5] G. Bastard, *Wave Mechanics Applied to Semiconductor Heterostructures* (Les Editions de Physique, Paris, 1990).
[6] G.A. Baraff and D. Gershoni, Phys. Rev. B **43**, 4011 (1991).
[7] M.G. Burt, J. Phys. Condens. Matter **4**, 6651 (1992).
[8] P. Butcher, N.H. March, and M.P. Tosi, *Physics of Low-Dimensional Semiconductor Structures* (Plenum, New York, 1993); H. Sakaki and H. Noge, *Nanostructures and Quantum Effects* (Springer-Verlag, Berlin, 1994).
[9] M. Cardona, N.E. Christensen, and G. Fasol, Phys. Rev. B **38**, 1806 (1988).
[10] M. Willatzen, M. Cardona, and N.E. Christensen, Phys. Rev. B **50**, 18 054 (1994).
[11] M.E. Flatte, P.M. Young, L.-H. Peng, and H. Ehrenreich, Phys. Rev. B **53**, 1963 (1996).
[12] R. Winkler and U. Rossler, Phys. Rev. B **48**, 8918 (1993).
[13] C.Y. Yeh, S.B. Zhang, and A. Zunger, Appl. Phys. Lett. **63**, 3455 (1993); Phys. Rev. B **50**, 14 405 (1994).
[14] L.W. Wang and A. Zunger, J. Phys. Chem. **98**, 2158 (1994); Phys. Rev. Lett. **73**, 1039 (1994); J. Chem. Phys. **100**, 2394 (1994).
[15] S.H. Wei and A. Zunger, J. Appl. Phys. **63**, 5794 (1988).
[16] D.M. Wood and A. Zunger, Phys. Rev. B **53**, 7949 (1996); D.M. Wood, A. Zunger, and D. Gershoni, Europhys. Lett. **33**, 383 (1996).
[17] A. Franceschetti, S.H. Wei, and A. Zunger, Phys. Rev. B **52**, 13 992 (1995).
[18] A. Franceschetti, S.H. Wei, and A. Zunger, Phys. Rev. B **50**, 8094 (1995).
[19] S.B. Zhang, C.Y. Yeh, and A. Zunger, Phys. Rev. B **48**, 11 204 (1993); A. Franceschetti and A. Zunger, Appl. Phys. Lett. **68**, 3455 (1996).
[20] C.B. Murray, D.J. Norris, and M.G. Bawendi, J. Am. Chem. Soc. **115**, 8706 (1993).
[21] Al.L. Efros and A.V. Rodina, Phys. Rev. B **47**, 10 005 (1993); A.I. Ekimov *et al.*., J. Opt. Soc. Am. B **10**, 100 (1993); Al.L. Efros, Phys. Rev. B **46**, 7448 (1992).
[22] L.W. Wang and A. Zunger, Phys. Rev. B **53**, 9579 (1996).
[23] A. Franceschetti and A. Zunger, Phys. Rev. B **52**, 14 664 (1995).
[24] J. Ihm, A. Zunger, and M.L. Cohen, J. Phys. C **12**, 4409 (1979).
[25] K.A. Mader and A. Zunger, Phys. Rev. B **50**, 17 393 (1994).
[26] L.W. Wang and A. Zunger, Phys. Rev. B **51**, 17 398 (1995).
[27] R.G. Dandrea and A. Zunger, Phys. Rev. B **43**, 8962 (1991).
[28] J.B. Xia and A. Baldereschi, China J. Semicond. **8**, 574 (1987); J.B. Xia, Surf. Sci. **228**, 476 (1989).
[29] In our plane-wave direct diagonalization, we only used $\sim$65 plane-wave bases, thus the eigenenergies are not converged in terms of the plane wave basis. However, as long as we use the same basis for the empirical pseudopotential band structure fitting and nanostructure calculation, its use is justified.
[30] P.O. Löwdin, J. Math. Phys. **3**, 969 (1962).
[31] In the empirical pseudopotential model of the GaAs/AlAs interface, the As atomic pseudopotential for the As atoms on the interface is an average of the As atomic pseudopotentials in the GaAs bulk and AlAs bulk (see Ref. [25]).
[32] ftp to ftp.nrel.gov as ''anonymous,'' then change directory to pub/sst/archive/MULTIBAND.K.P, and download all the files in that directory.

[33] S. Froyen (unpublished).
[34] To save memory, in the evaluation of Eq. (41), $H_A^{\mathrm{tot}}(p'k',pk)$ was not stored for all $(p'k',pk)$. Rather, $H_A^{\mathrm{tot}}(p'k',pk)$ can be calculated for each k' at a time; thus it does not need a large memory to store it.
[35] K.A. Mader and A. Zunger, Phys. Rev. B **51**, 10 462 (1995).
[36] K.A. Mader, L.W. Wang, and A. Zunger, J. Appl. Phys. **78**, 6639 (1995).